www.czasopisma.pan.pl PAN www.journals.pan.pl
Opto-Electronics Review 27 (2019) 174–193

Contents lists available at ScienceDirect

Opto-Electronics Review

journal homepage: http://www.journals.elsevier.com/opto-electronics review

Review

Recent infrared detector technologies, applications, trends and development of HgCdTe based cooled infrared focal plane arrays and their characterization

R.K. Bhan*, V. Dhar

Institute of Defence Scientists and Technologists, CFEES Campus, Brig SK Mazumdar Road, Timarpur, Delhi, 110054, India

ARTICLE INFO

Article history:
Received 16 January 2019
Received in revised form 1 April 2019
Accepted 26 April 2019
Available online 12 June 2019

Keywords:
Infrared detectors
Thermal imaging
HgCdTe
Cooled infrared detectors
Readout integrated circuit
Mid wave infrared
Focal plane arrays
Infrared applications

ABSTRACT

Infrared thermal imaging, using cooled and uncooled detectors, is continuously gaining attention because of its wide military and civilian applications. Futuristic requirements of high temperature operation, multispectral imaging, lower cost, higher resolution (using pixels) etc. are driving continuous developments in the field. Although there are good reviews in the literature by Rogalski [1–4], Martyniuk *et al.* [5] and Rogalski *et al.* [6] on various types of infrared detectors and technologies, this paper focuses on some of the important recent trends and diverse applications in this field and discusses some important fundamentals of these detectors.

Contents

* Corresponding author.
E-mail address: bhan_rk2003@yahoo.com (R.K. Bhan).

https://doi.org/10.1016/j.opelre.2019.04.004
1230-3402/

1. Introduction

It is well known that infrared (IR) focal plane arrays (IRFPAs) are widely used in military applications like night vision, reconnaissance, surveillance, missile guidance, etc. whereas civilian applications include remote sensing, firefighting, security, pollution-monitoring, leak-testing, etc. Further, these IRFPAs have medical applications in thermography, cancer and tumor detection, etc. Similarly for industrial applications they are used in nondestructive testing, process monitoring, etc. Although there are good reviews by Rogalski [1–4], Martyniuk *et al.* [5] and Rogalski *et al.* [6] and other workers in the literature focused on various types of infrared detectors and the technologies, this paper reviews some of the important recent trends and diverse applications along with associated basic principles of these detectors. In particular, some of the recent trends and new applications along with concepts that we feel will dominate in the future are discussed.

IRFPAs using hybrid focal plane array technology is the most preferred approach. In this case, the detector array and the readout integrated circuit (ROIC) are two separate entities hybridized together using an advanced indium bump interconnection technology (Fig. 1). For example, the HgCdTe (MCT) detector array and the ROIC are connected by an indium bump array, which provides an electrical, mechanical and thermal connection between the two arrays.

The hybrid architecture FPA is responsible for signal photon detection, selecting and transmitting required optical wave band for optical signals, and multiplexing of signal from parallel in to serial out. In action, the focal plane is illuminated with infrared

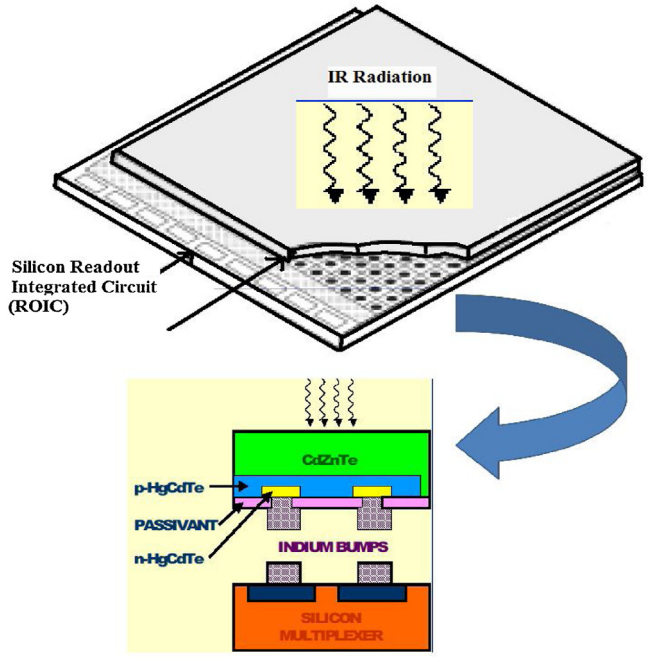

Fig. 1. The hybrid architecture of IRFPA consisting of HgCdTe based detector array that is bonded to Silicon CMOS ROIC using Indium bump technology.

background and signal; the optical input is filtered and then captured by the detectors for conversion to electrical signal which is then joined to the multiplexer through the interconnect indium bump technology. For utilizing the dynamic range (DR) of ROIC effectively, background suppression of the signal is required. The output video driver of the ROIC generates a serial video signal that contains all the useful information within the field of view (FOV) of the FPA that is a solid angle through which a detector sees the scene or is sensitive to IR radiation. The advantage in this type of architecture is that after selecting the best detector and best ROIC, they can be mated for hybridization process and similarly second best detector can be mated to second best ROIC and so on. In addition, in hybrid FPAs nearly all the incident photons are absorbed leading to hundred percent fill factor. The real estate area on the ROIC chip can be also best utilized in this configuration of IRFPAs compared to monolithic approach. The detailed progress in the development of hybrid IRFPAs including HgCdTe based detectors is given in a focused review by Rogalski [1–4], Martyniuk *et al.* [5], Rogalski *et al.* [6] and Kubiak *et al.* [7]. An excellent review on HOT infrared photodetectors is given in Ref. [8] wherein authors discussed how the limitations of slow responding thermal uncooled detectors can be overcome by HOT detectors using new barrier structures such as nBn, material. Martyniuk *et al.* [9,10] discussed the status of infrared barrier detectors and pointed out that certain solutions from these detectors have emerged as possible competitions to HgCdTe photodetectors. Another strategy for HOT infrared photodetectors is to include alternate materials such as type-II superlattices where dark current reduction is achieved via a concept of a photon-trapping detector [11]. Detailed analysis of the detector's performance was reported in Ref. 11. It was shown that these detectors have emerged as the competitors of HgCdTe photodetectors.

2. Review of recent trends, requirements and applications

2.1. Recent trends in detector

The recent major trends in Infrared are mainly happening in following aspects of infrared sensors: a) smaller pixels and larger FPAs, b) high operating temperature (HOT) devices–up to 120 K or above with same noise equivalent temperature difference (NETD) as at the canonical operating temperature of 80 K c) high dynamic range (HDR) imaging d) higher frame rates e) multispectral (MSI) / hyper-spectral imaging (HSI) and image fusion, on-chip processing (edge & motion detection, segmentation, etc.) – to reduce data overload. In addition some developments are taking place in digital FPAs, active pixels and foveas/region of interest (ROI), 3D range-gated imaging and curved FPAs. Since IR has always been driven by applications, further trends in IR will relate to artificial intelligence.

IR promises 'any time, any place imaging': day or night and all weather – but the last does not really happen: cloud, fog, rain, dust storms do affect the performance of these sensors. In addition, IR is used in many places: land (mostly), air, marine, outer space, even underground – everywhere except underwater. Image fusion of different IR bands and other sensors will help in improving the performance further. Furthermore, size, weight and power consumption (SWaP) are the guiding force for the market

and end users. As of now IR detector systems (barring uncooled microbolometers and InGaAs SWIR detectors) are bulky, heavy and consume a lot of power relative to visible cameras. There are three major approaches to SWaP: a) go to high operating temperature (HOT) devices, saving on cooling requirements leading to reduced dewar size and low power consumption, b) opt for curved flexible FPAs which suffer less distortion and need fewer lenses, and c) use small pixels and oversampling technology. Further, emerging requirements include improved ranges in various atmospheric conditions with recognition ranges >20 kms for airborne platforms.

According to Rogalski [12] next generation IR photon detectors will have: larger numbers of pixels (large format arrays with low non-uniformity), higher frame rates >250 Hz, better thermal resolution (1̃ mK), multicolor detection (3–4 bands) with low crosstalk (both spatial and spectral), on-chip processing (edge and motion detection, segmentation, etc.) – to reduce data overload, near room temperature operation to reduce power consumption by getting rid of the dewar and cooler, to increase reliability and reduce complexity but with lower specific detectivity, alternate substrates for affordable larger format IR FPAs. A further wish-list consists of a) high dynamic range (HDR) operation, b) polarization sensitivity, c) super-pixels, foveas or adaptive FPAs, and d) curved FPAs.

One of the fundamental figure of merit of infrared detectors is about the minimum infrared incident detectable power they can detect that is called as noise equivalent power (NEP). It depends on the energy distribution of the source; the amount of background radiation or thermal background and the detector material property and may be design parameters.

The NEP expressing a particular set of measurement conditions may be written as follows:

$$\mathrm{NEP}(500^{\circ}\mathrm{K}, 800\,\mathrm{Hz}, 5\,\mathrm{Hz}) = P_W A/(S/N). \quad (1)$$

The parameters in brackets of Eq. (1) LHS are the blackbody temperature, modulating frequency, and bandwidth, respectively; on RHS, *S* and *N* represent signal and noise, *A* the detector area, and P_W the radiant power density which reaches the detector from the blackbody. Smaller NEP signifies a better detector. Generally, as a practice, generally big represents better, the reciprocal of NEP called the detectivity *D* is often used for making useful comparison with similar other detectors. Further, detectivity is often normalized to an amplifier bandwidth of 1 Hz and a detector area of 1 cm^2 and leads to the parameter D^* such that:

$$D^* = (S/N)/P_W(\Delta f/A)^{1/2}. \quad (2)$$

The logic for normalization is that noise is proportional to square root of amplifier bandwidth and that *D* is inversely proportional to the square root of detector area.

One of the limits to the performance of IR photon detectors is given by the diffraction limit on pixel size. The spread of the diffraction-limited point spread function (PSF) is approximated by the diameter d of the first null of the airy disk and is given by: $d/2 = 1.22\lambda F\#$ where λ is the wavelength and F# is the f-number of the optics. Further, the background-limited infrared photodetector (BLIP) limit to detectivity D^* - applicable at different operating temperatures is given by Eq. (3) as follows:

$$2\eta e^2 Q_B >> 4\,kT/(R_0 A). \quad (3)$$

Where A is the detector area, R_0 is the resistance at zero bias (the product R_0A is a detector figure of merit), η is the quantum efficiency, T the temperature and Q_B the background photon flux. The authors of Ref. 13 already demonstrated 80% of BLIP for an 320 × 256 HgCdTe (MCT) LWIR FPA for mean D*.

The BLIP temperature is one of the important figure of merit for infrared researchers. For a given scene temperature and field of view, it is that operating temperature of the detector where dark current equals the background photon current. Figure 2 shows the

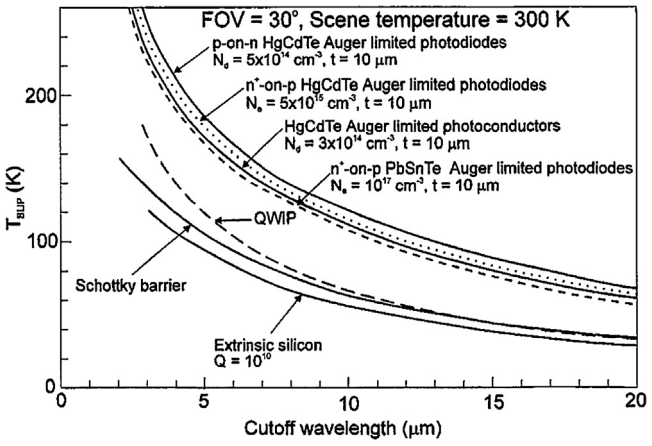

Fig. 2. Calculated temperature needed for BLIP operation *vs.* cutoff wavelength with 30◦ FOV and 300 K scene temperature for HgCdTe, QWIP, Schottky barrier and extrinsic silicon detectors (after Ref. 14).

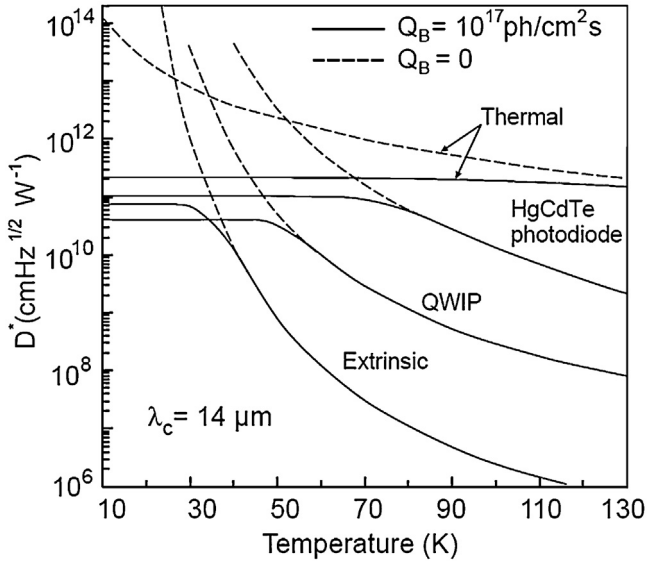

Fig. 3. Ideal limit of specific detectivity D^* as a function of temperature for long wavelength photon and thermal detectors with cut-off wavelength at 14 μm for background photon flux of zero and 10^{17} photons $cm^{-2}s^{-1}$ (after Ref. 16).

curves of estimated temperature required for BLIP operation *vs.* cutoff wavelength with 30◦ FOV and 300 K scene temperature [14] where N_a or N_d are dopant carrier concentration and t is the detector thickness. The figure shows that this temperature for the case of HgCdTe IR detectors is more than for the other types of photon detectors. Further, one can see that HgCdTe detectors with BLIP performance can operate with thermoelectric coolers at 5 μm, but 8 μm–12 μm detectors need ≈ 100 K operation temperature. Additionally, HgCdTe detectors show a higher operating temperature vis-à-vis extrinsic, Schottky barrier and QWIP detectors [15].

The ideal plot of D^* *vs.* temperature for background photon flux of zero and 10^{17} photons $cm^{-2}s^{-1}$ for 14 μm cut-off wavelength for different photon and thermal detectors is shown in Fig. 3 [16]. It can be clearly seen from this figure that at all range of temperatures, D^* of HgCdTe detectors is higher than extrinsic and QWIP detectors. Further, HgCdTe detectors with BLIP performance can work for T near 80 K or lower whereas extrinsic detectors operate at 30 K or lower and similarly QWIP requires 50 K or lower. It may be noted that $D^*_{th} > D^*_{ph}$ for $Q_B = 0$ & $T_{op} > 50$ K and for all temperatures when $Q_B = 10^{17}$ photons $cm^{-2}s^{-1}$.

Also it may be seen from this figure that ideal D^* for the thermal detectors is lesser tem**pe**rature dependence compared to the

photon detectors. Also for $Q_B = 0$ and $T_{op} < 50$ K, thermal detectors have lesser D^* values compared to photon detectors whereas for T_{op}>60 K, the limit favours the thermal detectors. At 300 K, the D^* performance of thermal detectors is higher than photon detectors. The above stated quantitative numbers will change with changing background, as is shown in Fig. 3 for a background of 10^{17} photons/cm^{2}s. It may be stated that the ideal curves of D^* for photon and thermal detectors show comparable fundamental limits at low temperatures.

Further, it follows from Fig. 3 that HgCdTe detectors have improved performance vis-à-vis QWIPs detectors in 35 to 77 K operating temperature but under 50 K HgCdTe detectors performance is somewhat limited by trap-assisted tunneling. In contrast, the QWIPs detectors have increases in the wider spectral range (below 14 μm) below 50 K with added advantage of the maturity of GaAs/AlGaAs technology that can yield high quality IRFPAs for many applications. It may be seen from this figure that the operating temperature for HgCdTe detectors is higher than QWIP and extrinsic detectors primarily because HgCdTe is characterized by high absorption coefficient and quantum efficiency and relatively low thermal generation rate compared to extrinsic detectors, silicide Schottky barriers and GaAs/AlGaAs QWIPs.

These relations are guiding principles for IR detectors. They suggest that a high D^* detector should convert the available photon flux (typically F#/2 optics) into a measurable signal without adding any noise more than input noise of background photons, with minimum power consumption and high operating temperature.

Some important applications for different wavelengths bands are listed below [17]:

a) SWIR (1–3 μm) systems are used to detect the bright rocket plumes of missiles in their boost phase.
b) MWIR (3–8 μm) systems are used to detect objects in space through booster burn-out against an Earth background.
c) LWIR (8–14 μm) systems are used to detect above-the-horizon objects against the background of cold space.
d) VLWIR (18–30 μm) systems are used to detect extremely cold objects against a cold space background, for exo-atmospheric conditions.

2.2. Si readout (ROIC) requirements and trends

The typical basic ROIC design (Fig. 4) using simple single transistor switch (STS) has changed since the 1990′s to the extent that STS has been replaced by some advances in per pixel signal conditioning circuitry like direct injection (DI), buffered direct injection (BDI), capacitive transimpedance amplifier (CTIA), or source follower (SF). Also reduction in pitch has been necessitated by matching ROIC ever reducing detector pitch due to demands of higher resolution. Due to advancement in CMOS technology, foundries offer technology nodes of around 10 nm at present. The function of the ROIC, as a multiplexer, is to capture light from IR sensor elements via indium bump connections for each and every pixel. It consists of a matrix of pixels, common buffer amplifiers, address registers and even an on-chip ADC for modern ROICs.

The advantages of using CMOS ROICs include: high signal handling capacity (SHC), high circuit density, small unit sizes (15 μm x 15 μm or less) desired in high density FPAs, low voltage, lower number of clocks, more uniform electrical characteristics and lower noise figures. These ROICs can tolerate lower R_0A diodes as compared to charge-coupled devices (CCDs), used in the 1990′s. The NMOS- and CMOS-switched readouts have been used for long (>1024 elements, linear), 15 μm element size linear and various 2D arrays (e.g., 128 × 128, 256 × 256, 320 × 256 and 640 × 512). These ROICs can provide the electronic shutter (snapshot, rolling shutter, non-destructive reads) and hence no mechanical shutter is required. In addition, they have low power consumption and can be radiation-tolerant (both by process and by design).

The modern ROICs' input signal conditioning (per pixel) circuits can have as high as 100 transistors and have functionality such as decoder based pixel addressing, windowing, sub-sampling and binning, digitally controlled bias, signal processing such as correlated double sampling, settable gain, noise filter, ADC and other logic functions (timing control, digital signal processing, etc.).

Further, CMOS ROICs use existing production oriented Si chip foundries (down to 0.13 μm technology node) and hence are cost affordable.

The important ROIC design Eq. is guided by Eqs. (4) and (5):

$$NETD = \frac{4F\#^2/(2t_I)^{1/2}}{\pi A^{1/2} D * \tau_{opt} \frac{dP_T}{dT_{amb}}}, \quad (4)$$

where F# is the f-number of the optics (f/D, f is the focal length and D is diameter), t_I is the integration time, A is the detector area, D^* is the detector specific detectivity, τ_{opt} is optics the transmission coefficient and P_T is the in-band power radiated by the target and T_{amb} is the ambient target temperature.

The integration time t_I is related to the SHC of the ROIC and the total detector current consisting of dark component I_D and I_{ph} and is given by:

$$t_I = 0.5q(SHC_{roic})/(I_{ph}+I_D), \quad (5)$$

where q is the electric charge. A high value of SHC is required to achieve longer integration time and, thus lower NETD at a given high frame rate.

Another way of estimating NETD is by given by Eq. (6) below [Ref. [2], Eq. (6)]:

$$NETD = 1/[C\sqrt{N}], \quad (6)$$

where C = 1/P (dP/dT) = differential contrast, $N = Q_B A t_I$ (i.e. SHC). It is obvious from this equation, that higher N leads to lower NETD. However, achieving larger N for a given frame rate (dependent in t_I) requires more pixel area A. For example in LWIR FPAs with 5 μm pixels it is difficult to integrate sufficient charge in such a small pixel knowing that state of- the-art storage density are of about 2.5×10^4 e$^-$ μm^{-2} only. Current ROIC design rules are just sufficient for tactical MWIR and LWIR ranges, for the pixel dimensions of 12 μm. This generally limits NETD to above 30 mK. Generally, 10^7 e's are required for reasonable SHC for a 5 μm unit cell. The vertical stacking of capacitors are being explored to solve these problems. Modern CMOS foundries carter to charge handling capacities of 2 fF μ m^{-2} in a 0.18 μm CMOS technology node. The use of CMOS manufacturing with smaller feature sizes will enable higher dynamic range for each pixel, as well as more advanced in-pixel processing [6].

Ultimately ROIC designed for photon detectors need to enable room temperature BLIP operation. This requires that the charge gathered from all directions (from the scene/target) during the integration time be completely captured by the ROIC capacitor - even while the pixel pitch shrinks to get better spatial resolution (since the capacitor size shrinks correspondingly).

The trend is for achieving low noise (<200 μV, high charge handling capacity (SHC)>10^8 e's per pixel that are needed for LWIR staring advantage to reach the NETD limit of 1 mK for terrestrial targets (T_{amb} ~300 K).

As regards the detector trends and requirements large signal levels, high quantum efficiency (QE) across spectral band (>80%), high response, low 1/f noise, better pixel uniformity, improved performance during haze, dusk and dawn conditions are the demands of the users. High responsivity such that signal » ROIC noise level, low noise levels and fast response (t ~msec), dark currents « 1 mA/cm^2 for

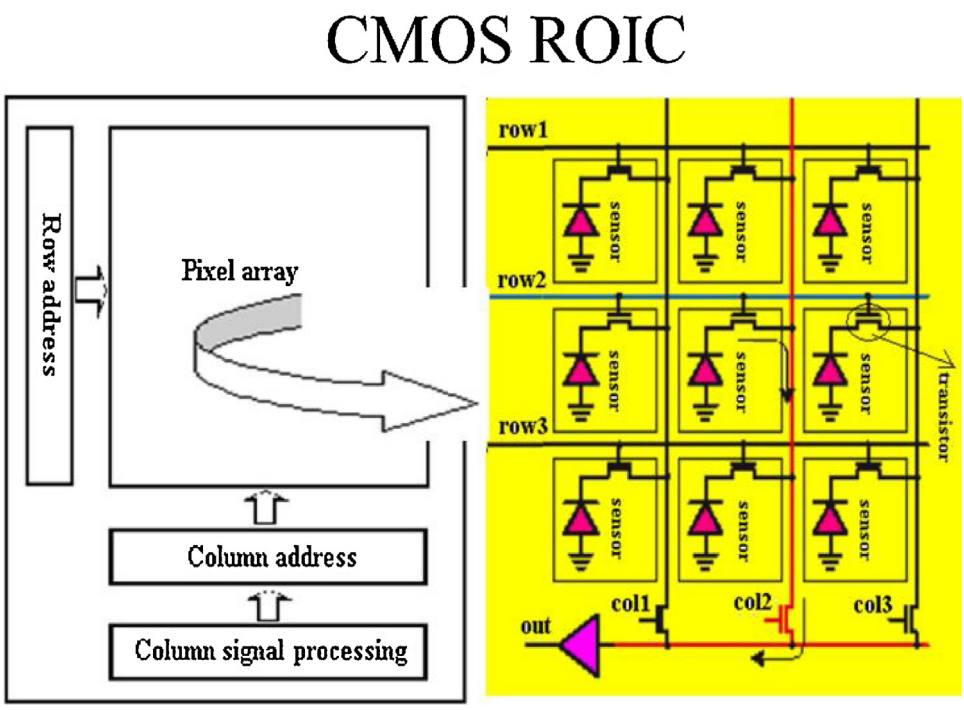

Fig. 4. Block diagram of typical CMOS ROIC depicting a 3 × 3 detector array size.

8–10 μm spectral (HgCdTe) [18] band and good linearity (>99.9%) are other requirements.

2.3. Detector requirements and trends

2.3.1. Emerging small pixel trends

Pixel sizes of the order of 10 μm have been proven in hybrid systems. However, the practice of reducing pixel sizes may continue in future. Since the diffraction-limited spot size is proportional to the wavelength (d = 2.44λF) [6]), it is easier to achieve small pixel sizes in systems that operate at shorter λ's: with low f-numbers (like f/1) d may be ˜ λ˜ 10 μm (in the LWIR). Oversampling – making pixels smaller than the diffraction limit - may deliver better resolution for larger pixels, but the benefit saturates quickly for smaller pixels (typical 4X oversampling is used in the MWIR). Reducing pixel size is essential for SWaP and cost reduction since the diameter of the optics goes down, and the size and weight of the dewar follow suit, and cooler power falls, but its lifetime and reliability improve. The pitch of 15 μm is in production today at Sofradir (France) and pitches of 10 μm and less are expected within a few years [see Fig. 5(a)] [19]. There is a similar tendency to reduce the pixel size of microbolometer arrays to achieve several potential benefits [see Fig. 5(b)] [20]. The details are given in Refs. [21–22].

Reducing pixel size also increases the detection and identification range of IR imaging systems, as does increased FPA array format (see calculated ranges in Fig. 6(a) for 25, 17, and 12 um pitch pixel of uncooled FPAs [21]. Choosing smaller pitch and larger format detectors, the detection range of an imager, with a fixed optical entrance aperture D_0, increases significantly. However, the detection range of many uncooled IR imaging systems is determined by their pixel resolution rather than by their sensitivity. In the inset of the figure the word 'CLEAR" refers to the use of 'clear weather conditions' in calculating atmospheric transmittance, which is needed in the NVTherm IP program to estimate the range. Raytheon has a heavy weapon thermal sight (HWTS) AN/PAS-13(V)3 $s^{-1}3$, which is a VOx microbolometer FPA: [23]. DRS also are developing HWTS [24].

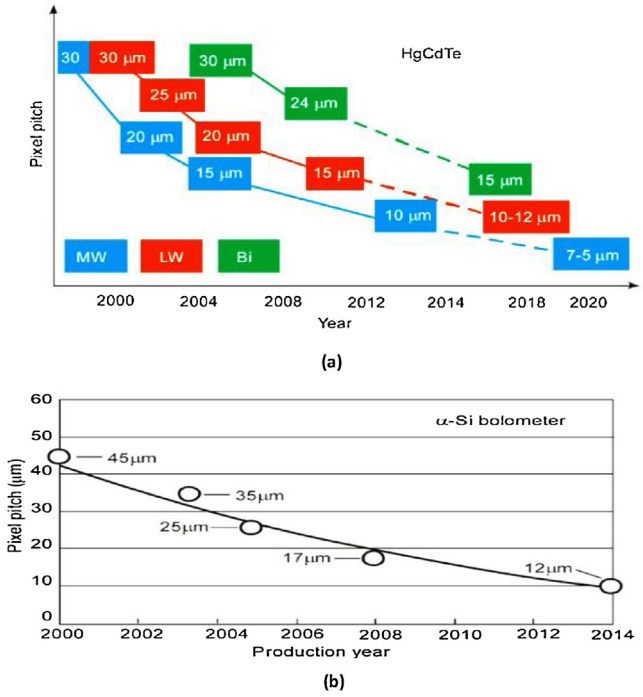

Fig. 5. Decreasing pitch of pixels as a function of year for (a) HgCdTe detector arrays (after Ref. 19) and (b) amorphous silicon microbolometers (after Ref. 20) as a result of manufacturing advancements.

Figure 6(b) illustrates the growth in detector size over the span of about fifty years [25]. Imaging FPAs formats have steadily become larger, driven by the increasing ability of CMOS technology and ROICs fabricated out of this technology to read and process array signals. FPAs nominally have the same growth rate as dynamic random access memories (DRAMs), with a doubling time of ĩ8 months (as per Moore's 'law'), but lagging by 5–10 years. The graph inserted in Fig. 6(b) shows n (where n is the number of pixels in MWIR sen-

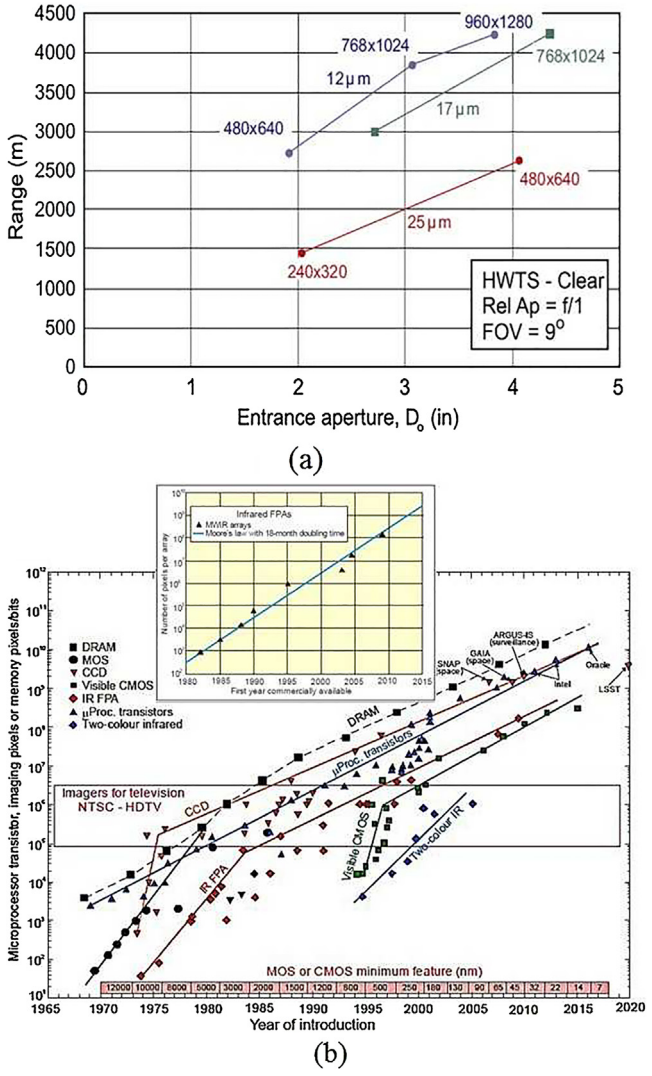

Fig. 6. (a) Simulation result of range *vs.* optics aperture for 25, 17, and 12 μm pitch pixel. The points for various detector array formats have been shown. It is that all the shown array sizes have 35 mK NETD (F#/1, 30 Hz) (after Ref. 21). (b)The growth in number of pixels as or transistor count a function of year for infrared imaging arrays vis-à-vis CMOS technology products such as transistors in visible CMOS imagers/microprocessors/CCD/DRAM etc. The associated CMOS design rules have also been depicted from 1970 to 2018 at the bottom. Inset on the top shows the comparison with Moore's law (After Ref [25].).

sor) as a function of the year initially for astronomy applications. Charge coupled devices (CCDs) having about 2 giga pixels are the largest available formats.

Array sizes still increase, but at a slower rate than expected from extrapolating Moore's Law, since market demand for better resolution is weak although the megapixel limit has been overcome. Optoelectronic arrays match the size of photographic film, replacing it for astronomy applications. Large format arrays improve the data rate for astronomy enormously; currently array sizes greater than 100 megapixels are available for these applications, and the largest arrays are being used for astronomy, not defense.

Further, the details of latest hybrid IRFPAs detector trends including array sizes and detector sizes of major manufacturers are given in Appendix 'A' following Ref. [25]. It may be seen from the table that highest array size of 4 K x 4 K with smallest pixel size of 10 × 10-μm have been demonstrated by Teledyne Imaging Sensors.

Since the cost of Ge optics, the standard IR material depends approximately upon the square of the diameter, decreasing the pixel size (for a given array format) lowers the cost of the optics. Alternatively, the reducing the pixel size allows more FPAs to be fabricated per wafer, bringing down processing costs. But the NETD is inversely proportional to the pixel area: reducing pixel size from 50 × 50-μm to 17 × 17-μm, would increase NETD by 9X – unless compensated for by improved electronics.

The important figures of merit that define the performance of an infrared detector are the modulation transfer function (MTF) and NETD. The MTF measures the fidelity (amount of blurring) of the imaging system in capturing spatial properties of the scene in the image. It is defined as the modulation ratio of the image and of the object as a function of the spatial frequency (cycles per unit length, cy/mm) of a sine-wave pattern of intensity. The system MTF is determined by the optics, detector, and display MTFs which are cascaded to obtain the MTF of the combination [26]: $MTF_{sys} = MTF_{opt}\ MTF_{det}\ MTF_{dis}$

Holst [27] showed that detector performance may be described in the spatial domain or in the (spatial) frequency domain. In the spatial domain, the optical blur diameter d_{blur} is compared with the detector size d_{det} : the ratio $d_{blur}/d_{det} = 2.44\lambda F/d_{det}$. i.e. this ratio is related to Fλ/d. Similarly, in the spatial frequency domain the optics cutoff f_{opt} is compared with the detector cutoff frequency f_{det}. The detector cutoff frequency f_{det} is given by $1/(2d_{det})$, and the optics cutoff frequency is given by $f_{opt} = 1/(\lambda F)$. So the ratio $f_{det}/ f_{opt} = \lambda F/d_{det}$.

One can show that the range approximation may be calculated by Eq. (7) [20]:

$$\text{Range} = (D\Delta x)/(M\lambda)(F\#\lambda/d). \tag{7}$$

For designers, modelling of NETD as a function of cutoff wavelength and given optic F# number, utilizing its the dependence of well capacity N_w, total current density (dark plus scene), photon flux density, integration time and detector quantum efficiency, it is useful to consider systems that are operating under the condition F#λ/d ≅, NETD is given by Eq. (8) [28]:

$$NETD = \frac{2}{C\lambda(\eta\varphi_B 2\pi t_I)}\left(\frac{F\#\lambda}{d}\right), \tag{8}$$

where *D* represents the optics aperture, *M* is minimum the pixel count needed for target Δ*x* identification, *C* is the scene contrast, *η* is the detector quantum efficiency, φ_B is the background flux into a 2π FOV, and t_I is the integration time. Equations (5) and (6) suggest that the parameter space defined by *F#λ* and *d* should be traded off for proper design of any thermal imaging system.

Figure 7 shows the design plot of detector pitch d *vs.F#λ*. It may be seen from this fugure that when the ratio $F\#\lambda/d \leqslant 0.41$ the performance is limited by the detector and if $F\#\lambda\ /d \geqslant 2$, the performance is limited by the optics as shown in Fig. 7. The implementation of design equation means $F\#\lambda/d = 2$ designer has to accommodate 4.88 pixels inside the Rayleigh blur circle. To maintain the same NETD, with changing optics or pixel pitch, the design values should lie on the lines having a constant $F\#\lambda\ /d$ [see Eqs. (5) and (6)]. In order to determine whether the detector or optics is limiting the performance, Figure 7 suggests that F-number of the optics has to be linked to pixel size or pitch.

The various types of detectors such as uncooled LWIR, cooled MWIR, cooled LWIR and Lamda scale LWIR manufactured by DRS Technologies have been evaluated experimentally and are shown in Fig. 7.

To overcome low sensitivity of microbolometers compared to photon detectors, bigger pixels sizes of more than 50 μm were used in the years before 1995. Lately however, with lower detector pitch, the optics continued to be ~*F#*/1 and hence uncooled systems moved from 'detector-limited' regimes to 'optics-limited' ones.

In summary, diffraction-limited optics having low F (e.g. F#/1) could benefit from pixels with pitch d ~ λ and oversampling may

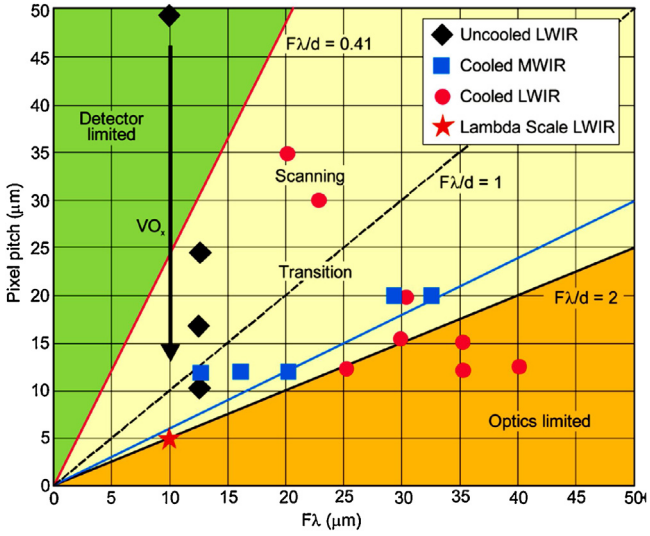

Fig. 7. *F#λ-d* space for infrared system design. The design plots of detector pitch d *vs F#λ* and experimental data points from DRS technologies uncooled LWIR, cooled MWIR, cooled LWIR and Lamda scale LWIR manufactured by DRS Technologies (After Ref. 26).

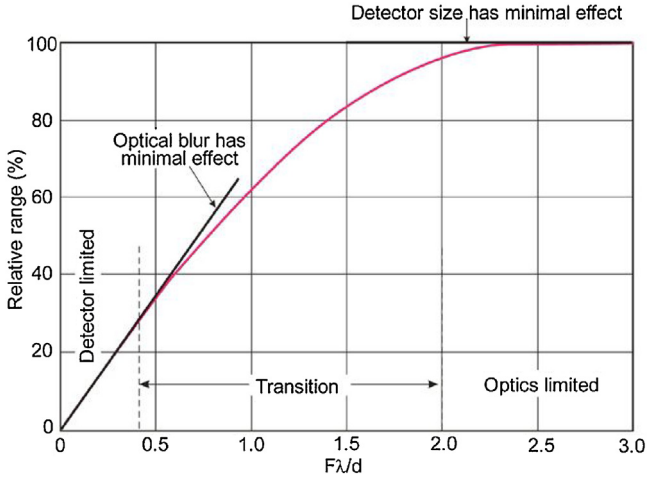

Fig. 8. Relative range as a function of *F#λ /d* (After Ref. 29).

provide additional resolution for smaller pixels but the benefits saturate quickly as pixel size is decreased. Present MWIR systems have pixel size of 10–12 μm corresponding to oversample of 4× and LWIR pixels are limited to 20 μm – but are shrunk further to use the same readout as MWIR FPAs. For F#/1 optics the smallest useful pixel size is of 2 μm for MWIR and 5 μm for LWIR, whereas for F#/1.2 optics the smallest useful pixel size is of 3 μm for MWIR and 6 μm for LWIR. Tradeoffs suggest that pixel size may be reduced to 5 μm for LWIR, both cooled and uncooled. For thermal detectors: 5–10 μm (LWIR).

As far as the range detection is concerned, the design of IR optics plays a crucial role and is very important. Holst and Driggers [29] have presented an important design curve of relative range (%) *vs*. F#λ /d shown in Fig. 8. If the performance of the system is limited by the detector, then reducing the detector size has a strong effect on range. In contrast to this, if the system performance is limited by optics, reducing the detector size has a little effect on range. Further, the range is lowered if the the atmospheric transmission and the NETD are included.

Recent calculations by Vallone *et al.* [30] on small-pitch HgCdTe photvoltiac detectors show that working on pixel pitches of smaller than cut-off wavelength will have many benefits in terms of lower volume, weight or cost. To determine the limit of pitch scaling in LWIR HgCdTe IRFPAs, 3D electrical and optical simulations for 3 μm, 5 μm, and 10 μm pitch were done. Results suggest that first neighbour cross talk was very small only for pixels with a 3 μm size and by using limited optical system.

Destefanis *et al.* [19] predict a 20% increase in detection range for d: 15→ 10 μm (for f/4 optics, MWIR MCT detector). Nowadays at Sofradir's HgCdTe foundry a pitch of 10 μm is easily manufactured with good yields, and pitches of <10 μm are scheduled in the short term (see Fig. 3(a) of Ref. [19]). The uncooled a-Si based microbolometers follow the same trend[(see Fig. 3(b)] [19].

Based on a 3D (optical and electrical combined) numerical simulation of LWIR MCT (x = 0.226) diodes with pitch d: 3,5 & 10 μm, crosstalk with first-neighbour pixels was controlled to less than 10% with pixel sizes of 3 μm and a diffraction-limited optical system, using a focused Gaussian beam on central pixel, as well as with uniform illumination. The calculated quantum efficiency (QE) *vs*. wavelength plots for p-on-n HgCdTe 3 × 3 pixel mini arrays showed peaks assigned to reflections from the internal metal contact surfaces for $\lambda \cong \lambda_c$.

2.4. Size, weight and power consumption (SWaP) requirements and trends

Near RT FPAs are needed to reduce power consumption, size and cost associated with cryo-coolers, and to increase reliability and life. Three approaches are being followed to reduce dark current in photodiodes (all essentially by Auger suppression): a) Exclusion/extraction in photodiodes using hetero-structures of HgCdTe diodes works only in MWIR and has troubles with 1/f noise that prevent imaging applications for many types of scenes, b) quantum dot infrared photodetectors (QDIPs) structures of GaAs/InGaAs using self-assembly have issues for control of growth, c) strained-layer superlattices (SLS) structures of InAs/GaInSb are still immature (passivation & material problems). However, a-Si, Vo_x and Ti-microbolometer FPAs provide RT operation, albeit with lower sensitivity, low frame rates and low f/#.

HOT IR FPAs deliver SWaP [31].The nBn MWIR FPA from Santa Barbara focal plane operates at 145 −175 K, dependent on ratio of scene to dark current demands. Their extended nBn design has a 14 μm cutoff and operates at 130–155 K with a performance equivalent to InSb FPA at 80 K, MCT FPA at 95 K, and epi-MCT at 115 K. This e-nBn FPA requires significantly smaller 2 W Stirling coolers instead of 6–12 W for a typical 640 × 512 format FPA. For a MWIR nBn sensor, in a 1280 × 1024 format, the 12 μm pixel pitch detector needs a 2.5 W cooler. The T2SLS Qmagiq 640 × 512 (20 μm pitch) FPA has a broadband spectral response from 3 to 11 μm, operates at up to 475 frames/s and can deliver a NETD of 8 mK for real-time 30 frame/s imagery. The wideband sensor enables a single thermal imager to satisfy the requirements of both MWIR and LWIR applications and promises to deliver on SWaP requirements.

Theoretical calculations indicate that parasitic and background currents limit the operation, otherwise a background radiation-limited LWIR HgCdTe detector with f/1 optics would yield a D* that is within $\sqrt{2}$ of BLIP at 215 K [32]. If one can reduce the background radiation by 66% by incorporating improved shielding methods, cryogenic cooling to 77 K can be given up and a single-stage TEC may be able to operate these detectors. However, for RT operation, background radiation has to be reduced by 90%. Achieving above increase in operating temperature may provide a noteworthy reduction in SWaP and costs for HgCdTe IDCAs and cameras for variety of applications.

Recently, uncooled thermal infrared sensors are finding a lot of applications with low range that demand low weight and size. Resistive microbolometers fabricated using advanced Si MEMS

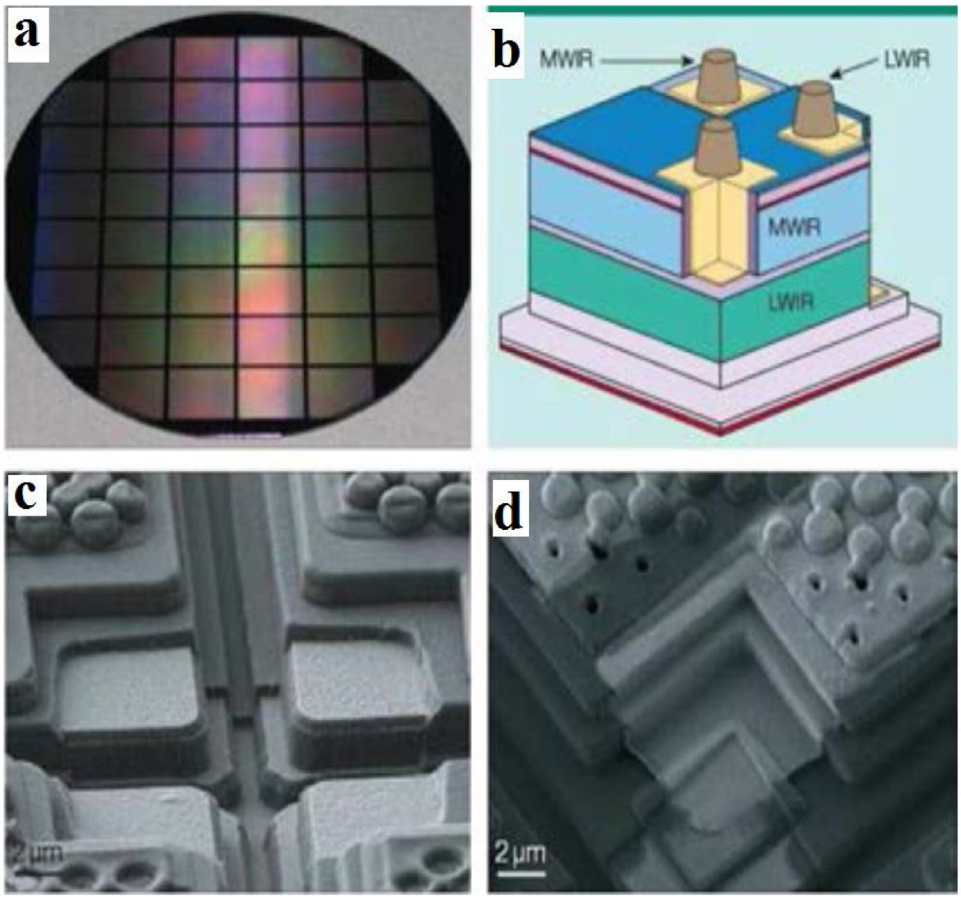

Fig. 9. Two-colour 320 × 256 MWIR/LWIR QWIP FPA: a individual dies as FPAs fabricated on a 4-in. GaAs wafer, b isometric three dimensional outlook of the pixel crossection, c SEM picture showing access and electrical connections for the common contact, d SEM picture showing that pixel connections are routed to the top of each pixel using the gold (after Ref. 36).

structures possess the highest sensitivity and the lowest pitch out of all uncooled detector types. The most important and leading two materials are vanadium oxide (VO_x) and amorphous silicon (a-Si) and many working IRFPAs have been demonstrated in research and production [33]. The comparatively low D* of the uncooled microbolometer arrays need low *f*-number optics˜*F*#/1.0 for majority of surveillance applications. These arrays become uncompetitive in both size and cost compared to photon detectors for the cases where focal length f > 200 mm is required. The slow frame rate and low sensitivity of these thermal detectors renders them less challenging to photon detectors. Presently most microbolometers operate upto 60 Hz frame-rate applications.

The trend is towards smaller pixel size which improves MTF and decreases response time and cost of the microbolometer FPA – but reduces FOV for given optics and may increase system noise. As regards pixel size and pitch, 10 µm seems to be the limit, particularly in the LWIR.

2.5. *Multi-spectral IRFPAs, image fusion and trends*

Multispectral IR provides target identification under conditions where one wavelength is unable to identify the target. Multispectral colour display helps in object recognition. Four colours may be maximum number of bands that can be stacked in a single pixel according to Norton [34]. However future trends and demands necessitate attempting almost all combinations of bands in short wave (SW), mid wave (MW) and long wave (LW) such as MW—MW, MW—LW, LW—LW, MW—MW—LW, MWLW-LW, LW—LW—LW, SW—MW—LW, etc.

Latest image fusion techniques combine the best of both images (e.g., high resolution of SW with temperature sensitivity of LW). Fusion has also been done between IR and some non-IR range like mm waves. Herve *et al.* [35] state that two colours are enough to simultaneously determine emissivity and temperature within 3% error. These authors presented an approach for measurement of the temperature and emissivity, by the use of infrared radiation. Unlike previous approaches, their methodology does not need a known surface emissivity. Their measurement involves measuring emissivity and temperature at the same time by measurement of changes in emitted radiation and surface related reflected infrared radiation, at two different spectral zones. This results in improved accuracy of the measured temperature particularly for situations where the surface optical properties vary while measuring it. Many experiments were done to validate the theoretical foundation, accuracy and limitations of the approach. The method has many industrial applications wherein temperature control of the mechanical parts is required such as in a lathe machine. The proposed method is easy to implement with low cost infrared and optical parts and reasonably accurate results are achieved.

Quantum well infrared photodetectors (QWIPs) are appropriate for the fabrication of simultaneously readable two-colour IR FPAs owing to their absorption in a very narrow spectral band because absorption outside of that band is negligible and almost transparent [36]. Hence, QWIPs give almost zero spectral cross-talk for any two spectral bands, if they are separated by a couple of microns in a wavelength. The vertical piling of growth layers is used for fabricating epitaxial QWIP layers. Such layers allow for a two-colour detection. Independent bias voltages are applied to each QWIP

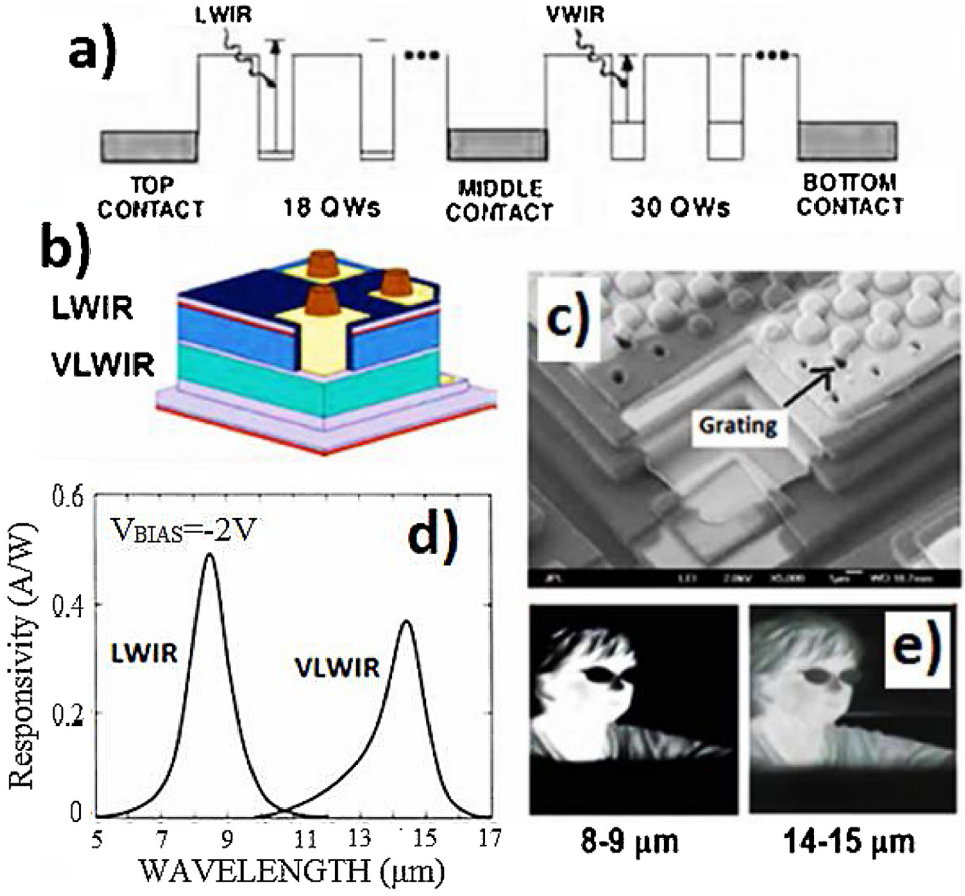

Fig. 10. a) Energy diagram of the LWIR (8–9 μm) sensitive and VLWIR (14–15 μm) sensitive two-colour infrared detector that utilizes the bound-to-continuum intersubband absorption, b) 3-D view of pixel structure, c) the electrical access connection to pixel are brought to the top using the gold metal, d) simultaneously measured spectral responsivity of vertically integrated LWIR and VLWIR dual band QWIP detector, e) a thermal image of the 8–9 and 14–15 μm two-color camera (After Ref. 37).

simultaneously through contact layers. Figures 9a and 9b show the full fabricated 4 inch wafer and cross-sectional view of the structure of a two-colour stacked QWIP reported from JPL with pixels collocated and simultaneously readable [36]. As depicted in Fig. 9b, the carriers emitted from each multi-quantum well (MQW) region are collected separately using three contacts where unmarked contact represents (see Fig. 9c) detector common contact. The electrical connections to the detector common and the LWIR connection are brought to the top of each pixel using via connections (See Fig. 9d).

At JPL, they have demonstrated functionality of 1024 × 1024 QWIP focal plane arrays (FPAs) on 4-inch GaAs wafers containing nine arrays using GaAs/AlGaAs based QWIP structures that can cover a very broad infrared (3–25 μm) region. They achieved a NETD of 22 mK and quantum efficiency of 2.5% in the wavelength range of 4.4–5.1 μm at a pixel pitch of 19.5 μm and operating temperature of 80 K and similarly achieved a NETD of 16 mK and quantum efficiency of 3.0% in the wavelength range of 8–9 μm at a pixel pitch of 19.5 μm and operating temperature of 72 K. As can be seen low quantum efficiency is the bottleneck in these detectors.

Gunapala *et al.* [37] reported prototype development of LWIR and VLWIR two-colour quantum well infrared photodetector (QWIP) device. The molecular beam epitaxy (MBE) growth was carried out on a three inch semi-insulating GaAs substrate. The fabrication of many 640 × 486 arrays in 8–9 and 14–15 μm two-colour (or dual wavelength) QWIP FPAs configurations was carried out. Those devices were then mated to matching 640 × 486 CMOS ROICs using flip chip indium bump technology. Followed by this, backside of the integrated device was thinned and substrate removed. Afterwards, hybrid FPA was mounted on a cold finger of a liquid helium cooled dewar for electro-optical characterization and demonstration of simultaneous two-colour imagery. The 8–9 μm detectors achieved BLIP performance at 70 K operating temperature for 300 K background with F#/2 cold stop. The 14–15 μm detectors also achieved BLIP at operating 40 K temperature under the same background conditions. Hence, these authors demonstrated dual band QWIP FPA in terms of quantum efficiency, detectivity, noise equivalent temperature difference (NETD), uniformity, and operability. Figures 10a) to 10e) show their results.

In short, these structures simultaneously detect thermal radiation at two wavelengths and can identify target by comparing two images detected at different wavelengths.

Gunapala *et al.* [38] also demonstrated functional IRFPAs using GaAs quantum dots (QDs). MBE growth technique was used for epitaxial growth of InAs–InGaAs– GaAsQDs. Growth by MBE allows to grow these large area layers with excellent uniformity and, hence well suited development of large-format LWIR IRFPAs. Dot-in-a-well (DWELL) structures do not suffer from normal absorption like in QWIP, instead it was demonstrated that it absorbs both 45° and normal incident light. Further, a reflection grating structure was added to enhance the quantum efficiency. The devices show peak responsivity out to 8.1 μm, with peak D^* touching 1×10^{10} Jones at 77 K. These InAs–InGaAs– GaAs quantum dots layers were the first of its kind and demonstrated a long-wavelength 640×512 pixel QDs infrared photodetector imaging FPA, with very good images and having noise equivalent temperature difference of 40 mK at 60-K operating temperature. Figures 11a) to 11d) show the results.

In summary, the advantages of these QDs are normal incidence detection, accurate control of quantum well width that is used for

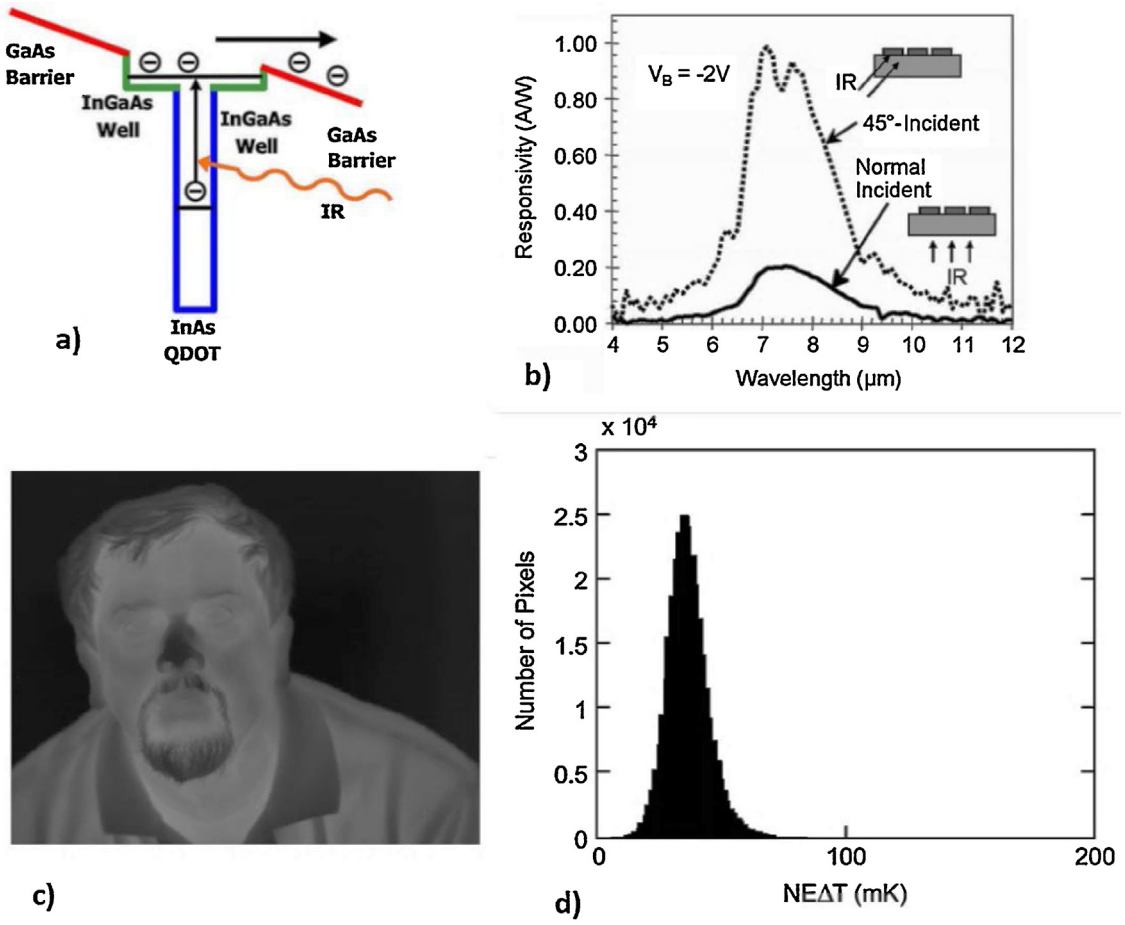

Fig. 11. a) The band diagram showing the principle of InAs–InGaAs– GaAs QDs dot-in-a-well (DWELL) infrared detector, b) the comparison of spectral responsivity for normal and 45 incidence, c) infrared image from a 640 × 512 pixels QDIP LWIR FPA using an f/2 AR coated germanium optics, d) NETD histogram of the 311 × 040 pixels of the 640 × 512 pixel QDIP FPA (After Ref. 38).

adjustment of spectral wavelength. The highest quantum efficiency obtained in a QDIP is 20% of absorption QE. Further, dual band FPAs can monitor both temperature and emissivity of the target. The polarization state of the target can be estimated and on-chip algorithms can extract information. These approaches can reduce size, complexity and cost of the FPAs.

2.6. *MEMS tunable IR detector*

Fabrication of compact integrated systems combining electronics, MEMS and photonics is a difficult task. All the three technologies have their limitations and boundaries within which they normally operate and guarantee performance and yield. However, once integrated, a lot of re-optimization process and re-design are needed to avoid the impact of one technological process step on the other technological step. This dual band AFPA technology having many advantages allows for a simultaneous collection of high-resolution MWIR infrared images, with spatially independent spectrally tuned imaging in the LWIR for improved target detection and classification.

Recent research developments in the field of MEMS-based tunable IR detectors can pave the way for development for multi-spectral IRFPAs based on voltage tuning. These technologies were developed and demonstrated in the framework of the adaptive focus plane array (AFPA) funded by DARPA. Current MEMS technological advances will easily allow fabrication of these structures and may be used for voltage based wavelength tuning.

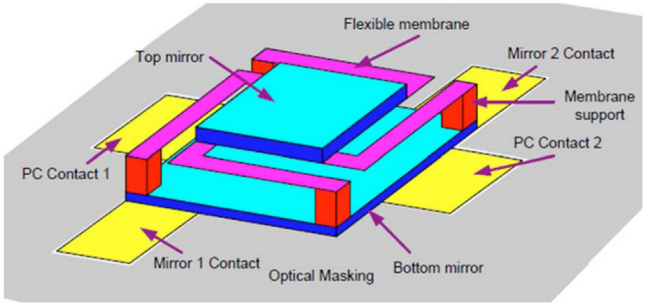

Fig. 12. Pictorial idea of MEMS-based tunable IR detector. The detector is placed under the bottom mirror (After Ref. 39).

Figure 12 depicts the idea of a MEMS based tunable IR detector. The MEMS filters are electrostatically actuated Fabry–Pérot tunable filters. Foundry fabrication of these MEMS filters is done by simple mounting process in such a way that the filters are facing toward the detector to minimize spectral cross-talk [39].

Using adaptive focal pane array in two bands, the concept of simultaneous spectral tuning (Fig. 13) in the LWIR region was demonstrated in Ref. 39. The reflective and ARC properties of optical coating were used for controlling spectral band pass and tuning range. The typical dimensions of MEMS filter were in range of 100 and 200 μm. However, using such a device requires a complex ROIC's per pixel circuitry for these improved functions.

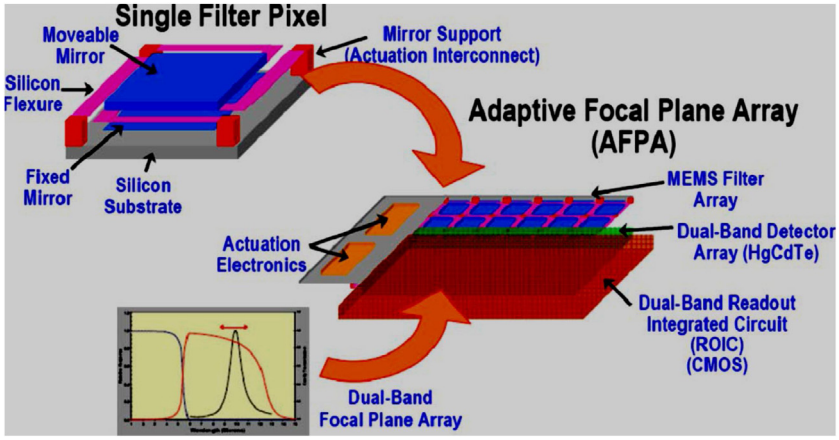

Fig. 13. Colour online dual band adaptive FPA (After Ref. 39).

Fig. 14. The effect of folded multiple capture for achieving high dynamic range. The three images are as follows: Top: image of HDR scene. Bottom left: simulated image with moving laser. Bottom right: simulated image using FMC with disturbance tolerance (After Ref. 42).

The MEMS tunable filter array (with 8×24 filters, 1 ms tuning speed) is integrated with a 640×480, 20 μm dual-band focal plane array: 8–11 and 3.5–5 μm. The filter air gap varies between 3.1–5.6 μm that allows Hyperspectral imaging (HSI) for an adaptive FPA that intelligently chooses wavelengths.

Krishna *et al.* [40] proposed FPAs that are spectrally tunable and wavelength agile. They invented a semiconductor detector with tunable spectral response. The detector structure includes an electronically tunable absorbing region that is based on inter-subband transitions of quantum states. Asymmetry in the absorbing region causes asymmetry in the local potential seen by carriers. As a result, the spectral response of the absorbing region can be tuned by changing a bias electric field in the region, typically achieved by changing a bias voltage applied across the region.

In short, the realization of the AFPA concepts and detectors with tunable spectral response offer the prospective for dramatic enhancements in serious military missions involving reconnaissance, battlefield surveillance, and precision targeting.

2.7. High dynamic range (HDR) and high frame rates' requirements and trends

In practical IRFPAs dynamic range (DR) is defined as the ratio of the maximum nonsaturating photocurrent to the smallest

Table 1
The emitted infrared radiation in terms of photon flux from scene temperature of 250 to 350 K in visible, MWIR and LWIR region along with corresponding contrast.

Spectral Band (μm)	Scene Temp.(K)			Contrast C (at 300 K)
	250 K	300 K	350 K	
0.4-0.7	10^8-10^{17}			0.2-8
3-5	1.8×10^{15}	1.5×10^{16}	7×10^{16}	0.045/K
8-12	2.4×10^{17}	6.2×10^{17}	1.3×10^{18}	0.02/K

detectable photocurrent or noise current. By this definition, we have $I_{max} = qQ_{sat}/t_I$ and $I_{min} = q\sigma_r/t_I$ where Q_{sat} is saturating well capacity of ROIC in number of electrons per well and σ_r is number of noise electrons in ROIC. Then, by this definition DR is defined as $DR = I_{max}/I_{min} = Q_{max}/\sigma_r$ where Q_{max} is maximum number of electrons that can be integrated without saturation.

Why do we need high dynamic range (HDR)? Most natural scenes (excluding fires, hot springs, volcanoes and man-made objects) lie in the temperature range of T: −50 °C to 50 °C and the corresponding photon fluxes in ph/cm^2/sec are given in Table 1 below.

As can be seen, photon flux varies by two orders of magnitude which demands and necessitates high dynamic range (HDR).

The effect and importance of requirement of high DR was studied by Kavusi and Gamal [41,42]. They proposed four different schemes viz. time-to-saturation, multiple-capture, asynchronous self-reset with multiple capture and synchronous self-reset with residue readout for achieving HDR. Further, they reported an improved scheme called folded multiple capture (FMC) by using by combining features of multiple capture schemes and the synchronous self-reset for achieving larger DR and high SNR at the high and low ends of the DR.

To demonstrate the effect and advantages of FMC, an image of a high DR scene (Fig. 14 top) is compared with same scene with an induced laser disturbance (Fig. 14 bottom left), as it would be captured by a conventional IRFPA. The third image (Fig. 14 bottom right) simulates the output after implementing FMC with a disturbance detection and applying correction. It may be clearly seen that the presence of disturbance is completely gone other than minor artifacts around the person and monitor.

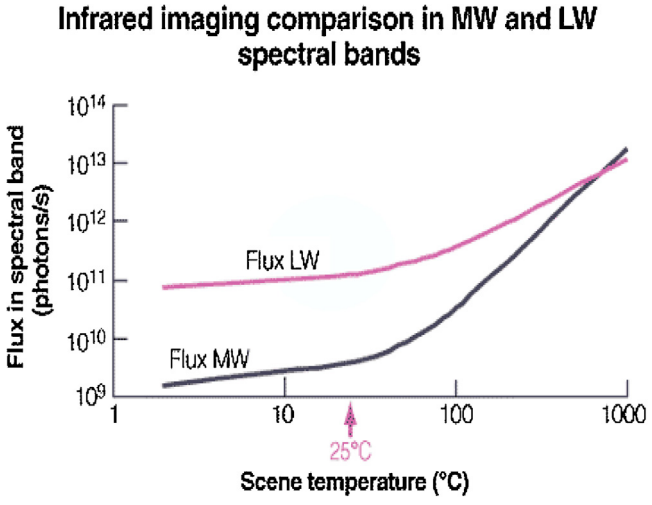

Fig. 15. Variation of photon flux with changing scene temperature for LWIR and MWIR range (After Ref. 43).

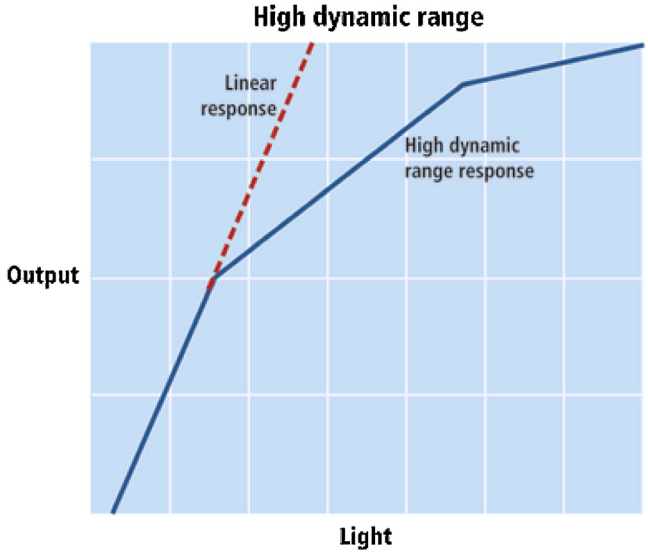

Fig. 16. Variation of typical IRFPA output as a function of input light or photon flux for a large range of dynamic range of the scene temperature (After Ref. 44).

LWIR is better suited to HDR than MWIR since a larger range of temperatures corresponds to a lower range of photon fluxes. This is depicted in Fig. 15 after Ref. 44. Such information is useful in selecting a wave band for applications like engines (IC, gas turbine, jet); rockets during launch and surveillance; or in thermal images that are obscured by fires/thermal camouflage. It may be mentioned here that consumer visible CMOS cameras use typically 54 dB DR whereas consumer CCD cameras use 66 dB DR. However, high end CCDs use DR > 78 dB. Smaller design rules of modern CMOS technology actually reduce SHC for smaller pixel sizes (due to lower integrating capacitor area associated per pixel) and lower operating voltages, which will reduce the DR – unless the noise floor is also decreased.

According to DARPA, modern defence applications require IR FPAs with >120 dB dynamic range to handle large variations in object radiance, sun reflections and laser jamming with 1000 frames/sec and 10 bit linearity.

Dynamic range (DR) is given by:

$$DR = 20\log(I_{max}/I_{min}). \quad (9)$$

To increase DR, we must either decrease I_{min} (i.e., noise floor) or increase maximum detector I_{max}, or try both. Since $I_{max} = qQ_{sat}/t_I$, it increases as t_I decreases for a given saturating signal handling capacity or well capacity Q_{sat} of ROIC. However, after including detector dark current noise contributions, total noise current I_{min} is given by $I_{min} = [(qI_D/t_I)^2 + (q\sigma_r/t_I)^2]^{1/2}$ where I_D is the detector dark current in electrons and σ_r is the noise of ROIC in electrons suggests that the dark current I_{min} decreases as t_I increases. This means that the integration time t_I has to be spatially adapted, i.e., short t_I for pixels that get high radiance, and long t_I for low radiance pixels.

In general, the output response of a typical IRFPA is not linear over the entire dynamic range of input light flux as shown in Fig. 16 [44]. Note that the output response is not linear over large input light or flux conditions and can be best approximated by two or three linear regions as depicted in this figure. The desired linear response is also shown. Actual experimental output may be best described by a two- or even three-degree polynomial.

As is the practice in visible CMOS imagers, the response can be tuned for either linear light response with approximately 55 dB of dynamic range or for high dynamic range response with as much as 100 dB of dynamic range as shown qualitatively in Fig. 16 showing

Fig. 17. Helicopter IR image captured using 1024 × 1024 MWIR FPA with fovea at center 64 × 64 pixels, while the rest of the image is of 16 × 16 super-pixels at a frame rate of 300 Hz (After Ref. 46).

two regions of linear responses. The same practice can be adopted in IRFPAs to cater for high flux LWIR applications [44].

According to the Weber-Fechner law, the eye response to a stimulus is logarithmic, which is roughly valid for radiance >100 cd/m^2. This means that a logarithmic sensor with HDR is needed, which can be obtained by logarithmic compression, using the sub-threshold characteristic of photodiodes given Eq. (10) by:

$$V_{out} = k\ln(I_{ph}/I_o). \quad (10)$$

A few decades of radiance are compressed into less than a volt – which means that subsequent circuits must be precise enough to extract the exact radiance (more bits needed).

Logarithmic sensors are ac-coupled so there is no offset as such; further the log means that the multiplicative gain term appears as an offset: i.e. single-point non-uniformity compensation (NUC) is sufficient to remove fixed pattern noise of a logarithmic sensor [38] *vs*. a 2-point NUC for a linear sensor.

There is always a tradeoff between high frame rate (HFR) IR imaging *vs*. high integration time (HIT).

Massie *et al.* [45,46] experimented with 1024 × 1024 MWIR image of a helicopter with a hi-res fovea at center of 64 × 64 pixels, while the rest of the image is low res at 16 × 16 super pixels, at a frame rate of 300 Hz - which allows imaging rotor and exhaust dynamics as shown in Fig. 17. Their experiments showed that higher integration time gives higher SNR and lower NETD and HIT may be a better option for high speed applications.

Recently, Telops [47] has announced a 256 × 256 MWIR InSb camera FAST-IR with 2000 frames/s (full frame) and 90,000 frames/sec with sub-windowing in an application note, studying muzzle flash (tank/artillery). The FAST-IR thermal imaging systems allow high-speed thermal imaging with a very good temporal resolution. They are, therefore, ideal to capture high speed dynamic events. These high performing thermal imaging cameras are also enormously sensitive, thus allowing the detection of difficult targets. Key benefits include up to 2000 fps at full frame and 90,000 fps in sub window mode in a 4-position filter wheel.

The concept of range-gated active imaging (or 3D imaging) is a well-known technique which was used for night vision enhancement in scattering environments. Many research workers demonstrated the performance enhancement of range gating. Gated IR imaging uses an active SWIR laser illuminator to increase the SNR as shown in Fig. 18. It can be used as a narrow field of view (NFOV) laser range gated (LRG) along with a passive uncooled wide field of view (WFOV) LWIR imager. This increases identification range. The wave band needed is the short wave (SW) band at 1.5 μm, 1.8 μm or 2 μm.

Christnacher *et al.* [48] demonstrated a short-wave infrared (SWIR) range-gated active imaging system that improved the penetration depth by a factor of 6.9 dense smoke. In contrast to this, combination of a short pulse with a short integration time gives better contrasted images in dense scattering media.

In order to satisfy the demands of long range IR imaging, detectors with response in nano sec range and having high SNR will be required. Since flux is proportional to inverse of distance square, there is requirement of gain for amplification of signal. The quest is to operate the detector near ambient temperatures. To satisfy the high resolution demands, large area detector arrays will be required to achieve true 3D imaging.

2.8. Flexible and curved IRFPAs

IR sensor systems would always demand for larger array FPAs with decreasing size and weight but it is tough to correct optical aberrations with bigger size of detector arrays and wide FOVs. The solution lies in flexible, spherical bio-inspired FPAs to correct optical aberrations and decrease use of many lenses in the optics of thermal imaging system.

Thinned membranes can be conformed to substrates for flat or curved focal planes to mimic the compound eye of the fly as shown in Fig. 19a) [49]. Such a configuration allows for one to eliminate optical elements, reduce mass and complexity as shown in Fig. 19b) [50]. Robust curved structures can be made out of GaN and alloys of thinned membranes. The curved focal plane array concept can be

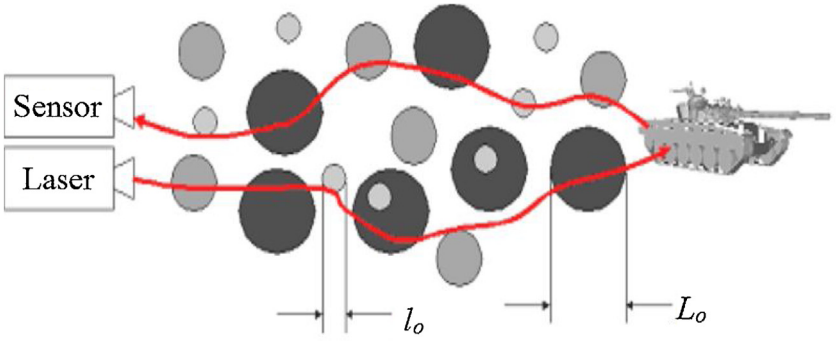

Fig. 18. Active laser illumination for range-gated active imaging (After Ref. 47).

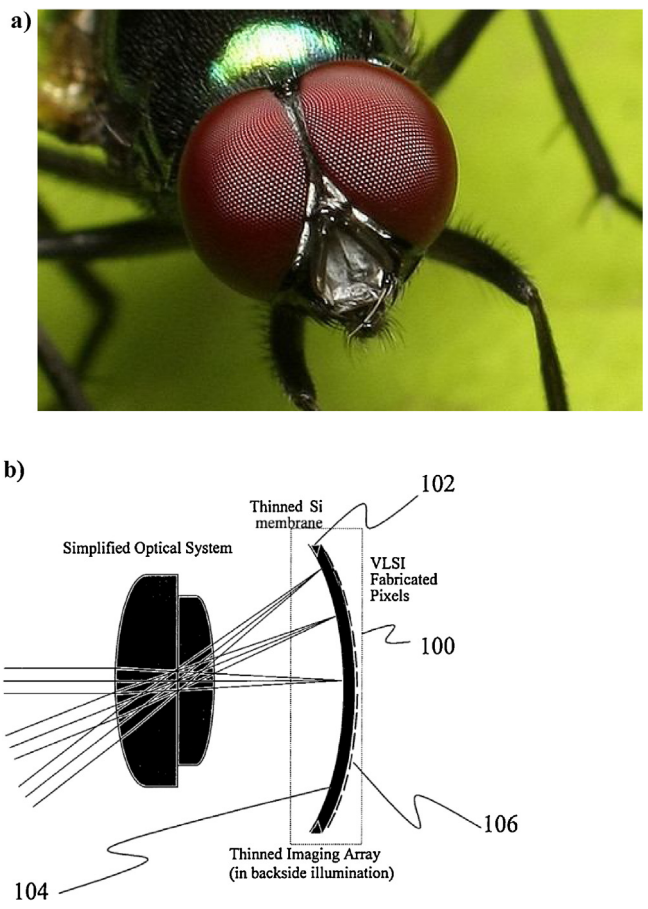

Fig. 19. a). Curved compound eye of the fly (After Ref. 49). b). Schematic of curved focal plane array (After Ref. [50]).

potentially made in III-N arrays; micron-size features in GaN have been fabricated using photo-electrochemical etching.

For many infrared field applications such as enhanced night vision, missile warning and telescopes the demand is reduce the weigh and size. These demands can be satisfied by use of flexible microelectronics technologies of FPAs with spherical curvature that can fix optical aberrations and decrease the use of multi lenses in cameras. The approach is based on motivation from curved compound eye of a fly. Tekaya *et al.* [51] demonstrated semicircular bowed cooled and microbolometers infrared detector arrays for compacted cameras.

An innovative process recipe was developed to be used for microbolometer detector arrays. An uncooled microbolometer 320×256 array with a 25 μm pitch was demonstrated having been thinned and curved as shown in Fig. 20. Its functionality was in tact after application of the innovative recipe on the FPA. The sensitivity of the FPA did not change much (<2.3% of mean response). On comparison of curved and flat FPAs using same number of lenses, MTF showed clear improvement in dispersion of optical rays.

Furthermore, another innovative process was developed for cooled hybrid HgCdTe IRFPAs having a radius of 550 mm. The cryogenic testing of this FPA at 80 K did not show in degradation in sensitivity vis-à-vis usual flat IRFPA.

2.9. Requirements for space and astronomy sensors

2.9.1. Use of IR sensors in space

Space and astronomy-based applications require distant objects (>100 kms) to be detected along with high SNR for faint sources and high quality material with no variability for tracking single pixel

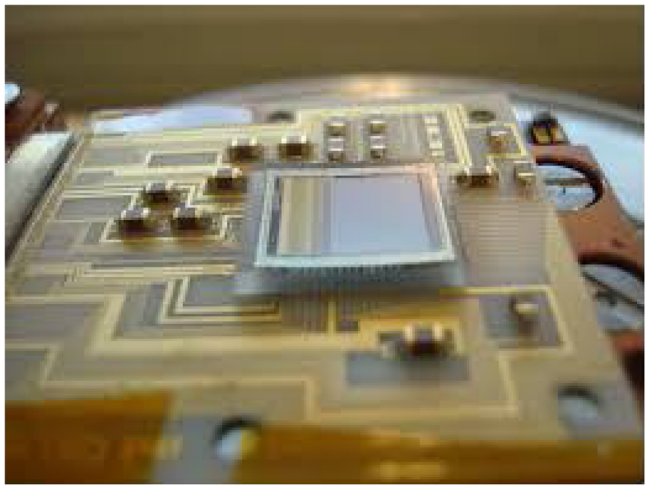

Fig. 20. A functional 256×320 25 μm pitch (roughly 1cm^2) uncooled FPA has been thinned and curved (After Ref. 51).

Fig. 21. Conceptual view of space based infrared (SBIRS) USA, which is nation's highest priority space program. (After Ref. 52).

objects. It is difficult to detect singe pixel objects. Further, space objects have low background photon flux (10^9 ph/cm^2/s). FPAs with low noise, operating at deep cryogenic temperatures of 40 K and low power consumption are required because power in space missions is limited. Added to this is low weight requirement for low launch cost, and radiation-hard devices are required to survive a flux of protons, gamma rays, etc.

Figure 21 shows the conceptual view of space based infrared (SBIRS), USA being the nation's highest priority space program [52]. SBIRS will provide technical intelligence to characterize infrared (IR) event signatures, phenomenology, and threat performance data, for strategic and operational combat commanders, the intelligent community and others. The satellite is equipped with around 1000 lb of infrared sensors. Mission control station receives data from all SBIRS sensors for further processing and manages the SBIRS constellation.

The space based missions are mainly for cold objects in bands VLWIR and beyond, electronically heated objects in MWIR and LWIR. Dim distant objects that require high efficiency detectors with optical signal amplification, moving objects requiring detectors with fast response time, large area detection/high resolution by large format detectors are being demanded for space-based applications. Additional capabilities require object identification by multi-colour and polarization sensing. Further the systems should be reconfigurable for use in multiple missions (space and earth backgrounds as well as manmade/natural/near/far objects). These types of applications require tunable detector response in

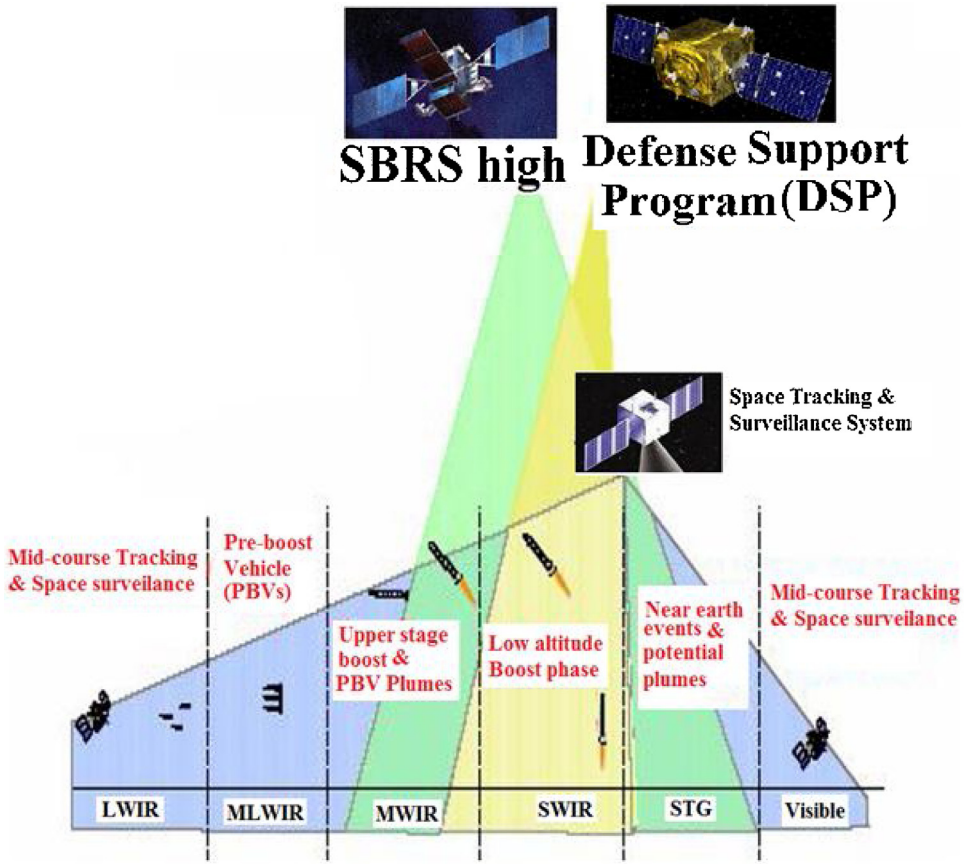

Fig. 22. Space-based infrared sensor systems (SBIRS) showing use of IR sensors in LWIR, MLWIR, MWIR, SWIR spectral bands in addition to visible spectral band. (After Ref. 53).

UV,Vis, IR, far IR, THz and radar. Further, advanced capabilities require small satellites, ultrafast processing, monolithic integration of detector / electronics / cooling, protection against harsh environments and the ability to reconfigure after damage.

Zheng *et al.* [53] argued that Type II superlattice (T2SL) is emerging infrared detector material for infrared astronomical space applications. Advantages of T2SL based detectors are high quantum efficiency, responsivity, detectivity, High uniformity and yield, mature III-V processing technology, large format arrays, multicolour operation, low Auger recombination rate, high temperature operation, low tunneling current, use band engineering and can be tuned from 3 to 30 μm by changing the thickness of the layers.

Figure 22 shows several space-based infrared sensor systems (SBIRS) in a high end Defense Support Program-DSP for strategic surveillance, Space Tracking and Surveillance System (STSS) positioned at different altitudes with variety of infrared sensors, each designed to observe a different target set. The STSS is an important project under the Missile Defense Agency, is a constellation of satellites in low-Earth orbits. It detects and tracks cold targets at a far distance. It requires sensors with large field of view for wide area coverage.

2.9.2. *Use of IR sensors in astronomy*

The IR is typically used to study objects which are cold (planets, Brown Dwarfs (BD): failed stars, 13–80 times Jupiter mass, M_{Jup}), dust embedded (young stellar objects, YSOs such as proto- or pre-Main Sequence stars) and behind dust (galactic center). There is an IR spectral window for this dust. Good IR observing sites are places that are dry, cold and high up (balloons, airplanes, mountains/plateaus, space). Brown Dwarfs (BDs) (type M,L) with temperatures T of the order of 3000-1500 K having λ_{pk} ~(1,2) μm whereas coolest BD (type T) of 800 K and λ_{pk} ~4 μm are studied using IRFPAs. An ultra-cool BD with temperature of 600 K was discovered by Wide-Field Infrared Survey Explorer (WISE). The thermal infrared imager, a 2D microbolometer FPA has been used for Hayabusa mission for imaging of near-Earth asteroid 162,173 Ryugu, for study of its surface thermal signatures. Further, Superhot exoplanet (WASP121b) (2700 K, 1.2 M_{Jup}) 900 light years away was also studied.

Astronomical objects called brown dwarfs are celestial bodies having intermediate size between a giant planet and a small star, believed to emit mainly infrared radiation because they do not have in built energy source and hence emit no visible light.

The spectrum of a brown dwarf (BD) peaks at longer wavelengths so it can be more easily seen at longer wavelengths [54] as shown in Fig. 23. The first BDs to be discovered had temperatures of 1,000–2,000 K and could only be detected in the IR. They were not hot enough to shine brightly in visible light. With more sensitive detectors, we are now able to detect brown dwarfs that are much cooler, and learning about these ultra-cool stars has become very important to understanding the formation of stars and planetary systems. The IR flux emitted by these BDs reaching earth is very small and can be detected only if it is within 100 light years.

The present and future largest format IR FPA for astronomy use 2 K x 2 K, 4 K x 4 K, 8 K x 8 K which are already under use or planned [1–6]. Owing to low dark currents and low noise besides excellent material uniformity, InSb photovoltaic detectors are preferred choice for infrared astronomy and applications using infrared telescopes. Lately, remarkable advancement has been made in the performance of InSb based FPAs. Additionally, InGaAs detectors have also been used for spectral bands between 0.9–1.7 μm and a high operating temperature. The results show that InGaAs detec-

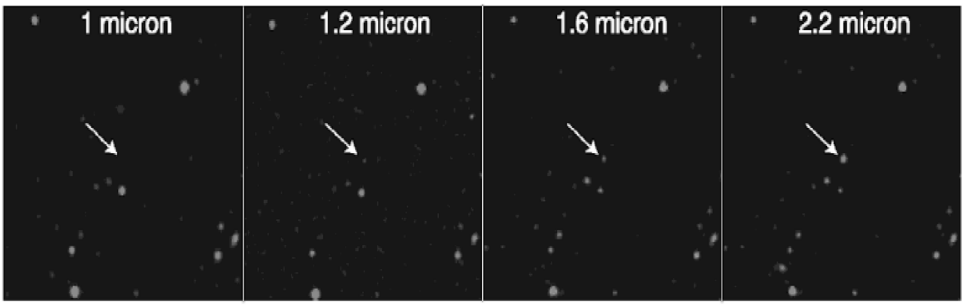

Fig. 23. A series of images of a brown dwarf star indicated by the arrow, at increasingly LWIR ranging from 1, 1.2, 1.6 and 2.2 um. Brown dwarf images peak at longer wavelengths (After Ref. 54).

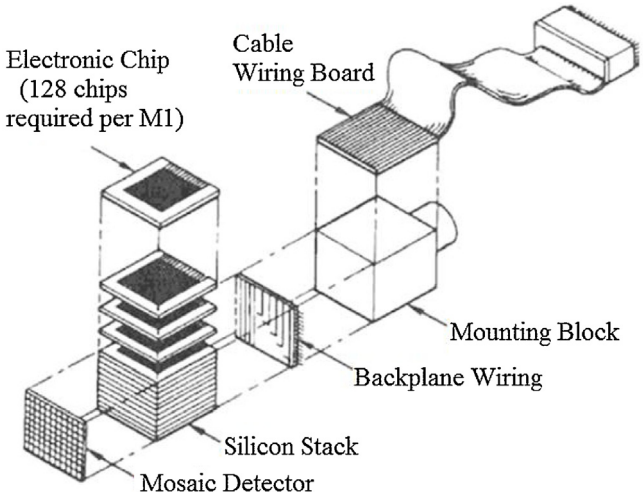

Fig. 24. A typical Z-plane 3D view of IRFPA proximity electronics (After Ref. 55).

tor technology is comparable to that of state-of-the-art HgCdTe imagers.

The high resolution requirement is of prime importance in astronomy applications. The detectors having 100 mega-pixels are being used currently for astronomy applications. High resolution IR detectors having better resolution than HDTV are available now.

2.10. 3D Z-plane IR FPAs proximity electronics trends

The video signal output from the IRFPA's dewar pin needs to be very close camera proximity electronics so that the limited drive capability of the video driver is not affected. This maintains high SNR besides inherent advantages in reducing system weight, power consumption and cost. The addition of more functions in per pixel circuitry like DI, BDI, CTIA, etc. makes ROIC more complicated to design and fabricate. This reduces the yield besides allowing less Silicon real estate per pixel resulting in low fill factor. It may stressed here CMOS designers cannot afford to put more circuits in pixel because they cannot reduce the vias beyond allowed design rules. In view of these difficulties and challenges, the obvious solution is to make the FPA a three dimensional unit and use the real estate behind optical surface for the processing electronics - analogous to the human (or the insect) eye. Figure 24 shows how Irvine sensors Corporation [48] implanted their three dimensional FPA and associated camera proximity electronics. Most of the electronic boards are located behind FPA in a stack. This minimizes video signal paths before it is digitized.

The Z-plane allows for a wide range of analogue processing including preamp, non-uniformity compensation (NUC, gain and offset), time-delay integration (TDI), spatial/temporal filtering, motion compensation, signal processing, etc. [55]. They (ISC) developed HYMOSS Z- plane 128 × 128 FPA buttable detector array with DR of 10^4 weighing 6 gms that consumes less than a watt of power. A 13 bit A/D requiring only 3 u W per channel at 1000 Hz was also developed for this project.

Are z-plane and curved focal plane technologies compatible (both together)? If not, which is more useful? This is the question which future research may ponder over.

2.11. Recognition based night surveillance

The preferred ability for any night vision surveillance and security applications demand true identification objects or even human faces. The mismatch between imagery from visible and infrared spectral bands is huge and due to this actual true identification of face is one of the difficult tasks and needs a lot of innovations and efficient algorithms as an integral part of the infrared imaging system.

The study of facial recognition by IR was done by Sarfraz and Stiefehagen [56]. Their deep neural network matches visible and IR images of a person with an accuracy rate of 80% assuming the image data base gives access to many visible images of the same person. The error or inaccuracy rate was as high as 45%, if only one visible image was used.

Facial recognition, being passive, can be used to identify a person without his or her knowledge (privacy issues!). With the advanced technological tools of today, no one can completely hide in darkness, thanks to facial recognition technology. The technology is based on study and analysis thermal signatures of human faces. However, the question is it may be just cheaper to just install a light and an ordinary Vis camera. The cost effectiveness of this technology may play a role here.

The images of human faces constructed from reflected daylight is appreciably different compared to infrared thermal signatures which keep on changing depending on the temperature of the skin, environment and even a person's expression as shown in Fig. 25. This makes it difficult to match infrared images with normal photos. Also, IR images tend to be of lower resolution than Vis images, making matching the two a challenge (the modality gap). It was found that the temperature of face is independent of skin colour, level of illumination or darkness. These infrared images are dependent facial expressions and emotional states.

Ayan Seal, PhD candidate at Jadavpur University Calcutta India has an algorithm for thermal signature of a face since the network of capillaries in each person's face is completely unique (although major arteries are similar) [57]. However, Seal's algorithm needs multiple images and does not work on moving subjects (so far).

In summary, such approaches have not been able to improve the modern advanced imaging systems by more than 10% in terms of basic or first rank identification. However, work is being pursued using artificial intelligence and pattern recognition methods in the IR community.

Fig. 25. Human face thermal signatures depend infrared signal that is skin temperature dependent, surroundings and expression of the face (After Ref. 56.

2.12. IR imaging and lie detection

Security agencies generally depend on finger prints and documents to establish the true identity of people. However, due to recent increased terrorist activities they are in need of technologies which use complementary and alternate techniques based on infrared imagery. Current research shows that by studying skin temperatures using IR cameras, fake identities can be isolated with acceptable level of errors.

In an experiment conducted by Warmelink *et al.* [58] at an international airport, skin temperature measurement was recorded using an IR imaging system while question about forthcoming trip was being asked. It was found that in case of truth tellers, there was no change in skin temperature compared to liars. Using this analysis, 64% of truth-tellers and 69% of liars were classified correctly. The actual results as per interviewers were 72% of truth tellers and 77% of liars.

The areas around the eye where the skin is thinner (the periorbital) and the cheeks are highly sensitive to temperature rise. When a person is being deceitful, their amplified brain activity is revealed in the face through unthinking facial expressions. The modern cameras can easily measure 0.1 K temperature resolution.

Applications for the above research for the suitability of IR imaging as a technique for lie detection at the airports may be envisaged in future. The problem, however, is that some truth-tellers may just be anxious, while habitual liars are not.

2.13. Spatial and spectral filtering on IRFPAs

Recently, night vision technologies are being developed for enhancing performance of IRFPAs by using spatial and spectral filters at the backside of hybrid detector arrays. Specially designed spectral filter masks for pixles of the detector arrays are pasted using a special glue with high alignment accuracy which leads to negligible cross talk between pixels and improved Nyquist frequency. Experimental demonstration of such systems was reported by Karni *et al.* [59]. Thee improvements may however be at the cost of marginal loss in quantum efficiency due to less than 100% fill factor.

2.14. Low light level imaging

In contrast to MWIR and LWIR, imaging in SWIR has distinctive benefits because it utilizes high irradiance IR flux and reflective imaging compared to conventional infrared imaging based on emissivity and less natural. The InGaAs/InP SWIR detector technology is foremost due to its low currents, high quantum efficiency and exceptional uniformity.

Harish *et al.* [60] reported SWIR images of a moonless night using low noise 640 × 512/15 μm InGaAs detector arrays and could detect a person at a distance of 140 m. They used a low cost, low weight and low power TEC based packaging. Software algorithms were designed for imaging from sub mlux to 100 Klux light levels. Figure 26 demonstrates the capability of the SWIR Imager to function as a vision enhancer in complete darkness on a moonless night.

In summary, trends suggest that SWIR has some unique advantages over Vis, NIR or thermal imaging. It benefits from relatively high irradiance level and intuitive reflective imaging from LLL imaging applications.

2.15. IR in strategic defence applications

J Ryu and S Kim [61] proposed a deep learning-based method called irYOLO using advanced real-time target recognition of UAVs by utilizing infrared images and field trainingand deep learning methods (DLM). Modern computer vision and DLM have proved to be very useful for detection of small drones. These authors developed a DLM by altering initial infared YOLO images. Such techniques will prove to be useful in preventing drone strikes.

The state-of-art, stealth plane needs the following functions in order to diminish its radar signature and thermal detection [62]:

- Decreasing thermal radiation from thrust
- Decreasing radar detection by changing some general shape (like introducing the split rudder)
- Decreasing recognition by radar when the aircraft opens its weapons bay
- Decreasing infra-red and radar detection during hostile climate environments.

Currently many modern US stealth warplanes have IR suppression. The B-2 bomber and F-22 /F-35 fighters use their internal fuel as heat sinks to cool outside skins. The fuel sucks up excess heat and improves the fuel efficiency. As you burn fuel during flight, you lose the ability to absorb heat internally so more heat radiates out of the tail pipe, where it is easily detected by an IRST (IR Search & Track). Planes are designed so that hot engines are not visible to ground IR systems – but the nose cone gets quite hot at high speeds allowing detection by enemy planes, and requires heat to be redirected sideways using thermal management. Similar considerations apply to tanks, whose engine heat must also be redirected sideways. Heating of the tank (ΔT) because of skin friction is small because the tank speed is small compared to the speed of sound sound v_s:

$$\Delta T/T_{amb} = (\gamma\text{-}1)M^2/2, \tag{11}$$

where the ratio of specific heats for air $\gamma = C_p/C_v \cong 1.4$, and M is the speed in Mach ($M = v/v_s$) [63,64].

In short, designers try to diminish the IR signature, but it is difficult to totally hide the heat signature of a sensor that is powered by hot fuel burning and pushing out of these gasses.

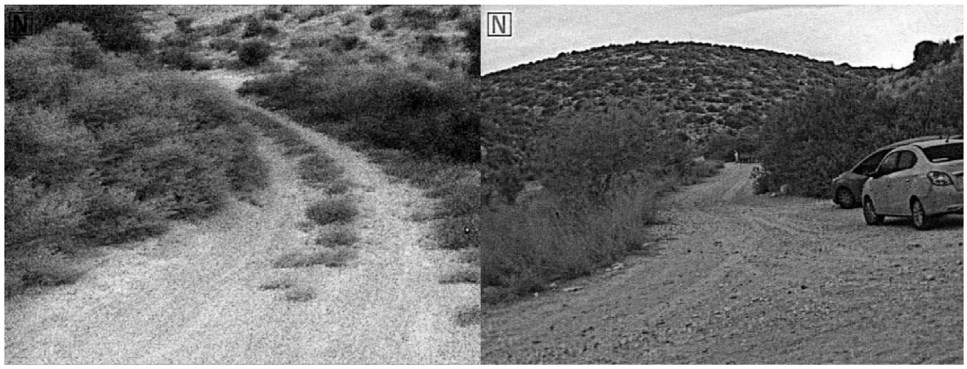

Fig. 26. Images taken on a moonless night with F/1.2, 32° field of view (FOV) optics. An image registered while driving at 10 km/h (Left); person waving detected at a distance of 140 m (Right) (After Ref. 60).

2.16. Augmented reality (AR) or artificial intelligence (AI) for IR imagery

There are some shortcomings and defects of IR images:

a) Low resolution compared with Vis and the solution lies to shift to SWIR band
b) Spatial non-uniformity, despite 2-point or 3-point fixed pattern noise (FPN) correction, it is worst in LWIR, better in MWIR, best in SWIR again solution lies to shift to SWIR band
c) IR imaging is non-intuitive and involves a strange combination of emissivity and temperature given by Stefan's law viz. $P \propto \varepsilon T^4$, however dP/dT, i.e., signal $S \propto \varepsilon T^3$ assuming all wavelengths from zero to infinity. In practice, according to Poropat [50] IR radiation propagates only in various bands (due to atmospheric absorption) leading to an increase in the exponent of the power law, i.e., $S \propto \varepsilon T^n$, where n>3 for bands. However, humans prefer natural imagery in visible that is reflectivity-dominated.

So, for a human observer, IR is only good for augmented reality (AR)! Areas in a scene will be designated with their emissivity ε, temperature T and range R (via range-gated IR or just a co-located IR laser range-finder). Range-gated IR would mean truly 3D imaging.

Also, from emissivity as a function of wavelength $\varepsilon(\lambda)$, what material the target is made of can be determined (in principle) but an AI may interpret MWIR, LWIR & VLWIR images better and faster than a human, since it need not be biased the same way.

2.17. Applications of next gen IRFPAs

The use for next generation of IRFPAs will include sensors that need no man intervention, easy to carry sensors, very small UAVs, missile warning seeker systems, and surveillance in all infrared spectral bands. Furthermore large array format IRFPAS grown by MBE growth techniques (or maybe by metallo-organic chemical vapour deposition, MOCVD) will include development of advanced large area IRFPAs for micro cameras with goals of : <4 gms weight, on-FPA processing, 130–150 mW power consumption, etc. The systems developed will have mission capabilities such as: battle/combat recce, metropolitan fighting, intelligence collecting, Special target reconnaissance etc.

2.18. Conclusions

It may be predicted that HOT HgCdTe technology will remain in the game because of its established fabrication houses and favorable and tunable properties. Since its spectral wavelengths can be tuned, this material will have its presence in almost all the spectral bands from short to very long wavelength bands. The technology will also keep on reducing the pitch of the detector arrays. In this context, uncooled microbolometers are being developed down to 5 to 10 um pitch in LWIR.

For achieving more integration times, for the same pixel area, signal or well capacity per unit area are required to be improved by innovations in integrating capacitor designs or else in fabrication technological capabilities.

The foundry houses which can provide low manufacturing costs will continue to exist because of huge demand.

Application for next generation of IRFPAs will include man-portable sensors, micro UAVs, ground/wall penetration, missile warning, missile seekers, multispectral Ssrveillance will keep the technology pushing to its limits.

Declaration of interests

The authors declare that they have no known competing financial interests or personal relationships that could have appeared to influence the work reported in this paper.

Acknowledgements

The authors would like to thank Chairman, IDST and Director, Solid State Physics Laboratory for their continuous support and for the permission to publish this work.

Appendix A. IRFPAs available from reputed vendors showing array size, pixel size, material and operating temperature (After Ref. [22])

Manufacturer/Web site	Size/Architecture	Pixel size (mm)	Detector material	Spectral range	Oper. temp.	D*(Jones) / NETD (mK)
Sensors Unlimited	320 × 256	12.5 × 12.5	InGaAs	0.7–1.7	300	12.9xE13
	320 × 256	25 × 25	InGaAs	0.4-1.7	300	<5E12
	640 × 512	25 × 25	InGaAs	0.7–1.7	300	4.2E13
	1280 × 1024	12.5 × 12.5	InGaAs	0.4–1.7	300	
Raytheon Vision Systems	1024 × 1024	30 × 30	InSb	0.6–5.0	50	23
www.raytheon.com/	2048 × 2048 (Orion II)	25 × 25	HgCdTe	0.6–5.0	32	

businesses/ncs/rvs/	2048 × 2048 (Virgo-2k)	20 × 20	HgCdTe	0.8–2.5	4–10	
index.html	2048 × 2048	15 × 15	HgCdTe/Si	3.0–5.0	78	
	1024 × 1024	25 × 25	Si:As	5–28	6.7	
	2048 × 1024	25 × 25	Si:As	5–28		
Teledyne Imaging Sensors	4096 × 4096 (H4RG)	10 × 10 or 15 × 15	HgCdTe	1.0–1.7	120	
http://teledynesi.com/imaging/	4096 × 4096 (H4RG)	10 × 10 or 15 × 15	HgCdTe	1.0–2.5	77	
	4096 × 4096 (H4RG)	10 × 10 or 15 × 15	HgCdTe	1.0–5.4	37	
	2048 × 2048 (H2RG)	18 × 18	HgCdTe	1.0–1.7	120	
	2048 × 2048 (H2RG)	18 × 18	HgCdTe	1.0–2.5	77	
	2048 × 2048 (H2RG)	18 × 18	HgCdTe	1.0–5.4	37	
Sofradir/	640 × 512	15 × 15	InGaAs	0.9-1.7	300	<18
www.sofradir.com/	640 × 512	15 × 15	InSb	3.7-4.8	80	18
	1280 × 1024 (Jupiter)	15 × 15	HgCdTe	3.7–4.8	77–110	<20
	1280 × 720 (Daphnis)	10 × 10	HgCdTe	3.4-4.9	110	≤16
	640 × 512 (Scorpio)	15 × 15	HgCdTe	1.5–5.1	<90	20
	640 × 512 (Leo)	15 × 15	HgCdTe	3.7–4.8	110	31
	640 × 512	20 × 20	QWIP	8.0-9.0	73	15–20
	640 × 512	24 × 24	HgCdTe	MW(dual)	77–80	20–25
	640 × 512/	24 × 24	HgCdTe	MW/LW(dual)	77–80	
Selex	320 × 256 (Saphira)	24 × 24	HgCdTe APD	0.8-2.5		17
www.leonardocompany.com	640 × 512 (Hawk)	16 × 16	HgCdTe	3–5	up to 170	
	1280 × 720 (Horizon)	12 × 12	HgCdTe	3.7-5		
	640 × 512 (Hawk)	16 × 16	HgCdTe	8–10	up to 90	32
	640 × 512 (CondorII)	24 × 24	HgCdTe	MW/LW (dual)	80	24/26
IAM	640 × 512	15 × 15	HgCdTe	1–5	95-120	17
www.aim-ir.com	640 × 512	15 × 15	HgCdTe	8–9	67-80	30
	640 × 512	20 × 20	HgCdTe	MW/LW	80	18/25
	384 × 288	40 × 40	Type II SL	MW(dual)	80	20/25
SCD	640 × 512	15 × 15	InSb	3-5		20
www.scd.co.il	1280 × 1024	15 × 15	InSb	3–5	77	20
	1920 × 1536	10 × 10	InSb	1-5.4		<25
	1280 × 1024	15 × 15	InAsSb nBn	3.6-4.2	150	20
	640 × 512	15 × 15	InAs/GaSb T2SL	λc = 9.5	80	15
FLIR Systems	640 × 512	15 × 15	InGaAs	0.9–1.7	300	1E10 ph/cm$\hat{2}$ s (NEI)
http://www.flir.com	640 × 512	15 × 15	InSb	3.4-5.2	80	<25
DRS Technologies	1280 × 720	12 × 12	HgCdTe	3-5		
	640 × 480	12 × 12	HgCdTe	3-5	7.8	20
	2048 × 2048	18 × 18	Si:As	5–28	7.8	25
	1024 × 1024	25 × 25	Si:As	5–28	7.8	
	2048 × 2048	18 × 18	Si:Sb	5–40		

References

[1] A. Rogalski, New material system for third generation infrared photodetectors, Opto-Electron. Rev. 16 (4) (2008) 458–482, http://dx.doi.org/10.2478/s11772-008-0047-7.
[2] A. Rogalski, J. Antoszewski, L. Faraone, Third-generation infrared photodetector arrays, J. Appl. Phys. 105 (091101) (2009) 1–44, http://dx.doi.org/10.1063/1.3099572.
[3] A. Rogalski, Recent progress in infrared detector technologies, Infrared Phys. Technol. 54 (2011) 136–154, http://dx.doi.org/10.1016/j.infrared.2010.12.003.
[4] A. Rogalski, History of infrared detectors, Opto-Electron. Rev. 20 (3) (2012) 279–308, http://dx.doi.org/10.2478/s11772−012−0037−7.
[5] P. Martyniuk, J. Antoszewski, M. Martyniuk, L. Faraone, A. Rogalski, New concepts in infrared photodetector designs, Appl. Phys. Rev. 1 (041102) (2014) 1–35, http://dx.doi.org/10.1063/1.4896193.
[6] A. Rogalski, P. Martyniuk, M. Kopytko, Challenges of small-pixel infrared detectors: a review, Rep. Prog. Phys. 79 (046501) (2016) 1–42, http://dx.doi.org/10.1088/0034-4885/79/4/046501.
[7] L. Kubiak, P. Madejczyk, J. Wenus, W. Gawron, K. Jozwikowski, J. Rutkowski, A. Rogalski, Status of HgCdTe photodiodes at the military university of technology, Opto-Electron. Rev. 11 (3) (2003) 211–226.
[8] P. Martyniuk, A. Rogalski, HOT infrared photodetectors, Opto-Electron. Rev. 21 (2) (2013) 239–257, http://dx.doi.org/10.2478/s11772−013−0090−x.
[9] P. Martyniuk, M. Kopytko, A. Rogalski, Barrier infrared detectors, Opto-Electron. Rev. 22 (2) (2014) 127–146, http://dx.doi.org/10.2478/s11772−014−0187−x.
[10] P. Martyniuk, A. Rogalski, MWIR barrier detectors versus HgCdTe photodiodes, Infrared Phys. Technol. 70 (2015) 125–128, http://dx.doi.org/10.1016/j.infrared.2014.09.026.
[11] W. Pusz, A. Kowalewski, P. Martyniuk, W. Gawron, E. Plis, S. Krishna, A. Rogalski, Mid-wavelength infrared type-II InAs/GaSb superlattice interband cascade photodetectors, Opt. Eng. 53 (4) (2014), 043107, http://dx.doi.org/10.1117/1.OE.53.4.043107 (1-8).
[12] A. Rogalski, Competitive technologies for third generation infrared photon detectors, Proc. SPIE. Infrared Technol. Appl. XXXI 6206 (1-15) (2006), 62060S, http://dx.doi.org/10.1117/12.666882.
[13] Philippe M. Tribolet, Philippe Chorier, Alain Manissadjian, Patricia Costa, Jean-Pierre Chatard, High-performance infrared detectors at sofradir, Proc. SPIE Infrared Detect. Focal Plane Arrays VI 4028 (2000) 438–456, http://dx.doi.org/10.1117/12.391759.
[14] A. Rogalski, Comparison of the performance of quantum well and conventional bulk infrared photodetectors, Infrared Phys. Technol. 38 (1997) 295–310, http://dx.doi.org/10.1016/S1350-4495(97)00015-7.
[15] A. Rogalski, HgCdTe infrared detector material: history, status and outlook, Rep. Prog. Phys. 68 (2005) 2267–2336, http://dx.doi.org/10.1088/0034-4885/68/10/R01.
[16] R. Ciupa, A. Rogalski, Performance limitations of photon and thermal infrared detectors, Opto-Electron. Rev. 5 (1997) 257–266.
[17] http://www.globalsecurity.org/space/library/report/1998/sbirs-brochure/part02.htm.
[18] M.A. Kinch, State-of-the-Art Infrared Detector Technology, SPIE Press, Bellingham, Washington, USA, 2014.
[19] G. Destéfanis, P. Tribolet, M. Vuillermet, D.B. Lanfrey, MCT IR detectors in France, Proc. SPIE. Infrared Technol. Appl. XXXVII 8012 (1-12) (2011) 801235, http://dx.doi.org/10.1117/12.886904.
[20] A. Hoffman, Semiconductor processing technology improves resolution of infrared arrays, Laser Focus World 42 (2) (2006) 81–84 https://www.laserfocusworld.com/articles/print/volume-42/issue-2/features/ir-detectors-semiconductor-processing-technology-improves-resolution-of-infrared-arrays.html.
[21] C. Li, G. Skidmore, C. Howard, E. Clarke, C.J. Han, Advancement in 17-micron pixel pitch uncooled focal plane arrays, Proc. SPIE Infrared Technol. Appl. XXXV 7298 (1-11) (2009) 72980S, http://dx.doi.org/10.1117/12.818189.
[22] http://www.sofradir.com/technology/mct/.
[23] http://www.nitevis.com/ANPAS-13E.htm.
[24] https://www.armyrecognition.com/april_2016_global_defense_security_news_industry/us_army_awards_raytheon_and_drs_$56_million_to_develop_next-gen_infrared_night_vision_50504163.html.
[25] A. Rogalski, Next decade in infrared detectors, Proc. SPIE Electro-Opt. Infrared Syst. Technol. Appl. XIV 10433 (1-25) (2017), 104330L, http://dx.doi.org/10.1117/12.2300779.
[26] J. Robinson, M. Kinch, M. Marquis, D. Littlejohn, K. Jeppson, Case for small pixels: system perspective and FPA challenge, image sensing technologies: materials devices systems and applications, Proc. SPIE 9100 (1-9) (2014) 91000I, http://dx.doi.org/10.1117/12.2054452.
[27] G.C. Holst, Imaging system performance based upon Fλ/d, Opt. Eng. 46 (10) (2007) 103204, http://dx.doi.org/10.1117/1.2790066 (1-8).
[28] M.A. Kinch, State-of-the-Art Infrared Detector Technology, SPIE Press, Bellingham, Washington, USA, 2014, pp. 24–29.

[29] G.C. Holst, R.G. Driggers, Small detectors in infrared system design, Opt. Eng. 51 (9) (2012) 096401, http://dx.doi.org/10.1117/1.OE.51.9.096401 (1-10).
[30] M. Vallone, M. Goano, F. Bertazzi, G. Ghione, W. Schirmacher, S. Hanna, H. Figgemeie, Simulation of small-pitch HgCdTe photodetectors, J. Electron. Mater. 46 (9) (2017) 5458–5470, http://dx.doi.org/10.1007/s11664-017-5378-z.
[31] A. Adams, E. Rittenberg, HOT IR sensors improve IR camera size, weight, and power, Laser Focus World 50 (1) (2014) https://www.laserfocusworld.com/articles/print/volume-50/issue-01/features/advances-in-detectors-hot-ir-sensors-improve-ir-camera-size-weight-and-power.html.
[32] D. Lee, M. Carmody, E. Piquette, P. Dreiske, A. Chen, A. Yulius, D. Edwall, S. Bhargava, M. Zandian, W.E. Tennant, High-operating temperature HgCdTe: a vision for the near future, J. Electron. Mater. 45 (2016) 4587–4595, http://dx.doi.org/10.1007/s11664-016-4566-6.
[33] M. Noda, Uncooled thermal infrared sensors: recent Status in microbolometers and their sensing materials, Sensor Lett. 3 (3) (2005) 194–205, http://dx.doi.org/10.1166/sl.2005.038.
[34] P.R. Norton, Infrared detectors in the next millennium, Proc. SPIE Infrared Technol. Appl. XXV 3698 (1999) 652–665, http://dx.doi.org/10.1117/12.354568.
[35] P. Herve, J. Cedelle, I. Negreanu, Infrared technique for simultaneous determination of temperature and emissivity, Infrared Phys. Technol. 55 (1) (2012) 1–10, http://dx.doi.org/10.1016/j.infrared.2010.09.001.
[36] S.D. Gunapala, S.V. Bandara, J.K. Liu, E.M. Luong, S.B. Rafol, J.M. Mumolo, D.Z. Ting, J.J. Bock, M.E. Ressler, M.W. Werner, P.D. LeVan, R. Chehayeb, C.A. Kukkonen, M. Ley, P. LeVan, M.A. Fauci, Recent developments and applications of quantum well infrared photodetector focal plane arrays, in: J. Rutkowski, J. Wenus, L. Kubiak (Eds.), Proc. SPIE Intl. Conference on Solid State Crystals 2000: Epilayers and Heterostructures in Optoelectronics and Semiconductor Technology 4413 (2001) 323–338, http://dx.doi.org/10.1117/12.425451.
[37] S.D. Gunapala, S.V. Bandara, A. Singh, J.K. Liu, S.B. Rafol, E.M. Luong, J.M. Mumolo, N.Q. Tran, D.Z.-Y. Ting, J.D. Vincent, C.A. Shott, J. Long, P.D. LeVan, 640/spl times/486 long-wavelength two-color GaAs/AlGaAs quantum well infrared photodetector (QWIP) focal plane array camera, IEEE T. Electron Dev. 47 (5) (2000) 963–971, http://dx.doi.org/10.1109/16.841227.
[38] S.D. Gunapala, S.V. Bandara, C.J. Hill, D.Z. Ting, J.K. Liu, Sir B. Rafol, E.R. Blazejewski, J.M. Mumolo, S.A. Keo, S. Krishna, Y.-C. Chang, C.A. Shott, 640 512 pixels Long-wavelength infrared (LWIR) quantum-dot infrared photodetector (QDIP) imaging focal plane array, IEEE J. Quant. Elect. 43 (3) (2007) 230–237, http://dx.doi.org/10.1109/JQE.2006.889645.
[39] W.J. Gunning, J. DeNatale, P. Stupar, R. Borwick, S. Lauxterman, P. Kobrin, J. Auyeung, Dual band adaptive focal plane array: an example of the challenge and potential of intelligent integrated microsystems, Proc. SPIE Intell. Integr. Microsyst. 6232 (1-9) (2006) 62320F, http://dx.doi.org/10.1117/12.669724.
[40] S. Krishna, J. S. Tyo, M. M. Hayat, S. Raghavan, U. Sakoglu, Detector with tunable spectral response, United States Patent, Patent No. US 7,217,951 B2, May15 2007.
[41] S. Kavusi, A. El Gamal, Quantitative study of High dynamic range image sensor architectures, SPIE 5301 (2004) 264–275, http://dx.doi.org/10.1117/12.544517.
[42] S. Kavusi, A. El Gamal, Folded multiple capture: an architecture for high dynamic range disturbance-tolerant focal plane array, in: Bjørn F. Andresen, Gabor F. Fulop (Eds.), Proc. of SPIE Infrared Technology and Applications XXX 5406 (2004) 351–360, http://dx.doi.org/10.1117/12.543543 (2204).
[43] C.J. Alicandro, Sensors Expand IR imaging Range, 2019 https://www.vision-systems.com/articles/print/volume-10/issue-6/features/component-integration/sensors-expand-ir-imaging-range.html.
[44] https://www.vision-systems.com/articles/print/volume-13/issue-8/features/product-focus/word-on-the-wire.html.
[45] M.A. Massie, J.T. Woolaway, J.P. Curzan, P.L. McCarley, Neuromorphic infrared focal plane performs sensor fusion on-plane local-contrast-enhancement spatial and temporal filtering, Visual Inf. Process. II Proc. SPIE 1961 (1993) 160–174, http://dx.doi.org/10.1117/12.150947.
[46] M.A. Massie, J.P. Curzan, P.L. McCarley, N.I. Rummelt, Imaging applications of large-format variable acuity super pixel imagers, Infrared Technol. Appl. XXXII Proc. SPIE 6206 (1-12) (2006) 62060Z, http://dx.doi.org/10.1117/12.668508.
[47] http://telops.com/media/documents/Telops%20General%20Brochure%202016_low_res.pdf.
[48] F. Christnacher, S. Schertzer, N. Metzger, E. Bacher, M. Laurenzis, R. Habermacher, Influence of gating and of the gate shape on the penetration capacity of range-gated active imaging in scattering environments, Opt. Express 23 (26) (2015), http://dx.doi.org/10.1364/OE.23.032897, 32987-32908.
[49] http://koziy.thelinebreaker.co/compound-eyes/http://koziy.thelinebreaker.co/compound-eyes/flies-compound-eyes-arthropod-eyes-are-called-compound-eye-flickr.html.
[50] https://patents.google.com/patent/US7786421.
[51] K. Tekaya, M. Fendler, D. Dumas, K. Inal, E. Massoni, Y. Gaeremynck, G. Druart, D. Henry, Hemispherical curved monolithic cooled and uncooled infrared focal plane arrays for compact cameras, Infrared Technol. Appl. XL Proc. SPIE 9070 (1-8) (2014) 90702T, http://dx.doi.org/10.1117/12.2049967.
[52] https://www.slideshare.net/hindujudaic/space-based-infrared-systemsbirs-usa-one-of-the-nations-highest-priority-space-programs.
[53] L. Zhenga, M.Z. Tidrowb, A. Novellob, H. Weichelc, S. Vohrad, Type II strained layer superlattice: a potential infrared sensor material for space, Proc. of SPIE 6900 (1-10) (2008), 69000F, http://dx.doi.org/10.1117/12.768420.
[54] D.L. Clements, Infrared Astronomy – Seeing the Heat: from William Herschel to the Herschel Space Observatory, CRC Press, Taylor and Francis Group, Florida, USA, 2015, pp. 93, ch. 4.5.
[55] J.L. Miller, Principles of Infrared Technology: A Practical Guide to the State of the Art, Van Nostrand Reinhold, New York, 1994, pp. 2012, ch 6.6.
[56] M.S. Sarfraz, R. Stiefehagen, Deep Perceptual Mapping for Thermal to Visible Face Recognition, 1507, Cornell University Library, arXiv, 2015, pp. 02879 https://arxiv.org/pdf/1507.02879.pdf.
[57] A. Seal, S. Ganguly, D. Bhattacharjee, M. Nasipuri, D.K. Basu, Automated Thermal Face Recognition Based on Minutiae Extraction, 2019 https://arxiv.org/abs/1309.1000.
[58] L. Warmelink, A. Vrij, S. Mann, S. Leal, D. Forrester, R.P. Fisher, Thermal imaging as a lie detection tool at airports, Law Human Behav. 35 (1) (2011) 40–48, http://dx.doi.org/10.1007/s10979-010-9251-3.
[59] Y. Karni, M. Nitzani, E. Jacobsohn, I. Grimberg, S. Gliksman, A. Giladi, L. Krasovitski, E. Avnon, I. Hirsh, L. Bikov, I. Lukomsky, L. Shkedy, R. Fraenkel, I. Shtrichman, P. Gonzalez, A. Lambrechts, Spatial and spectral filtering on focal plane arrays, infrared technology and applications XLIV, Proc. SPIE 10624 (1-10) (2018), 106241H, http://dx.doi.org/10.1117/12.2299302.
[60] I. Hirsh, E. Louzon, A. Aharon, R. Gazit, D. Bar, P. Kondrashov, M. Weinstein, M. Savchenko, M. Regensburger, A. Navon, E. Shunam, O. Rahat, A. Mediouni, E. Mor, A. Shay, R. Iosevich, M. Ben-Ezra, A. Tuito, I. Shtrichman, Low SWaP SWIR video engine for image intensifier replacement, Proc. of SPIE Infrared Technol. Appl. XLIV 10624 (1-9) (2018) 1062406, http://dx.doi.org/10.1117/12.2303705.
[61] J.H. Ryu, S. Kim, Small infrared target detection by data-driven proposal and deep learning-based classification, Infrared Technol. Appl. XLIV Proc. SPIE 10624 (1-10) (2018), 106241J, http://dx.doi.org/10.1117/12.2304677.
[62] http://aviation.stackexchange.com/questions/16876/how-do-stealth-aircraft-reduce-the-heat-signature.
[63] V.A. Kurganov, http://www.thermopedia.com/content/291/.
[64] H.O. Toft, Simplified Aerodynamic Heating of Rockets, Aug., 2014 http://dark.dk/documents/technical_notes/simplified%20aerodynamic%20heating%20of%20rockets.pdf.